Journal of Computational Acoustics, Vol. 12, No. 3 (2004) 319–354

INTERNATIONAL ASSOCIATION
FOR MATHEMATICS AND
COMPUTERS IN SIMULATION

PROPAGATION OF ACOUSTICS WAVES OF NONSIMPLEX FORM IN A MATERIAL WITH HYSTERETIC QUADRATIC NONLINEARITY: ANALYSIS AND NUMERICAL SIMULATIONS

V. ALESHIN

Laboratoire d'Acoustique, UMR – CNRS 6613, Faculté des Sciences, Université du Maine, av. O. Messiaen, 72085 Le Mans, France
Interdisciplinary Research Center, Kathoieke Universiteit Leuven, (Campus Kortrijk), Etienne Saabelaan 53 8500 Kortrijk, Belgium
aleshinv@mail.ru

V. GUSEV

Laboratoire de Physique de l'Etat Condensé, UMR – CNRS 6087, Faculté des Sciences, Université du Maine, av. O. Messiaen, 72085 Le Mans, France
vitali.goussev@univ-lemans.fr

V. YU. ZAITSEV

Institute of Applied Physics, Russian Academy of Sciences, Uljanova St. 46, 603950, Nyzhnyi Novgorod, Russia
vyuzai@hydro.appl.sci-nnov.ru

Received 26 May 2003
Revised 26 September 2003

The numerical scheme for the analysis of the acoustic wave transformation in materials with nonlinearity hysteresis and end-point memory is developed. Both numerical and analytical predictions are obtained concerning mixing of a wave at fundamental frequency (ω-wave) and a wave at doubled frequency (2ω-wave) in the materials with hysteretic quadratic nonlinearity. The observed wave spectrum broadening is found to be in qualitative agreement with the selection rules for the multiphonon processes in this type of materials. The predicted transformation of an initially complex wave (with four extrema over a period) into a simplex wave (with two extrema over a period) in nonlinear propagation is found to be one of the manifestations of the nonlinear hysteretic absorption. It is demonstrated that at short propagation distances the interaction of the ω- and 2ω-waves is mainly through the mechanism of the nonlinear hysteretic absorption and is not strongly influenced by the process of higher harmonics generation and their inverse influence on the input waves. The regimes of the induced and self-induced transparency are predicted. The influence of the transition from the simplex wave to complex wave emission (or vice versa) on the processes of the induced absorption and transparency is identified.

Keywords: Hysteresis; nonlinear acoustics; two frequency mixing induced transparency; induced absorption.

1. Introduction

Stimulated by pioneer acoustic experiments in vibrating metallic rods[1,2] there is still a stable interest to the investigation of the nonlinear wave phenomena in materials exhibiting hysteresis in their nonlinear properties. The nonlinear acoustic experiments conducted in different type of materials (including, for example, polycrystalline metals,[1–4] rocks[5–8] and ceramics[9]) lead to the conclusion on the universality of the observed nonlinear acoustic effects in the sense that they are characteristic of a large class of micro-inhomogeneous materials.[2,10] An additional term "mesoscopic" for the notation of these materials has been introduced quite recently.[10] This term emphasizes that the acoustic nonlinearity of the material is due to some mechanical features in its structure, which are significantly bigger than the interatomic distances, but significantly smaller than the acoustic wavelength. Hysteresis in the strain–strain relationship is, however, only one feature of a rich variety of remarkable nonlinear properties of micro-inhomogeneous (mesoscopic) materials.[8,11–13] Another fascinating feature is the property of these materials to memorize their mechanical (acoustical) loading history.[14,15] For example, the current behavior of the material depends on the magnitude of the latest extremum in the stress/strain history, furthermore, some of the other extrema in the loading/unloading history are also memorized (the end-point memory[16–19]). In particular, the material always remembers the extremum previous to the latest one, as well as the absolute maximum and the absolute minimum of the loading history.

Both the end-point memory and the nonlinearity hysteresis can be successfully phenomenologically modeled using the so-called Preisach-Mayergoyz (PM) space formalism.[16–18] This is a mathematical tool elaborated by Krasnoselskii[19] for a physical model proposed by Preisach for magnetic hysteresis.[16] A theorem important for the representation of actual hysteresis nonlinearities by Preisach's model was proven by Mayergoyz.[17,18] In the PM-space approach it is assumed that the response of a material to external excitation is a linear superposition of the individual responses of hysteretic mesoscopic mechanical elements (see the next section for the details).

In the theoretical analysis of the nonlinear acoustic phenomena in the framework of the PM-space phenomenology the mathematical complexity is caused rather by the memory effects than by the hysteresis in nonlinearity. If the acoustic wave (incident on a mesoscopic material) induces sufficiently simple loading history then complete analytical description of the nonlinear wave evolution is possible.[20–22] Exact analytical solutions are obtained[20–22] for the so-called "simplex" waves,[23] i.e. periodic waves with a single maximum and a single minimum over a period. Qualitatively this became possible because there were only two end-points (extrema) to be kept in memory during wave profile transformation. If an acoustic wave contains over a period additionally to the absolute extrema also some local ones ("complex" wave[23]), then the problem of memorizing and erasing of the end-points in the process of wave propagation becomes hardly tractable analytically. Here is exactly a point where numerical modeling should help us in understanding the fundamental laws of the nonlinear wave interactions in mesoscopic materials.

In the present paper we develop a numerical scheme for the evaluation of the nonlinear propagation of an arbitrary acoustic signal and present the results of this simulation for the initially biharmonic signal. The acoustic wave at the boundary is composed of two harmonic waves at a fundamental (ω) and doubled (2ω) frequency. We simulated the nonlinear transformation of the wave profile for different relative amplitudes and phases of the initial waves at ω and 2ω as well as the transformation of the frequency spectrum of the total wave. Our results indicate an important contribution of the forth harmonic (4ω) to the spectrum of the signal. The transformation of a complex wave into a simplex wave in the nonlinear propagation is demonstrated and the dependence of the process on the relative phase of the ω- and 2ω-waves is explained. Peculiar regimes of the induced transparency (where the increasing amplitude of the $\omega(2\omega)$-wave leads to fall in the absorption of $2\omega(\omega)$-wave) are predicted both numerically and analytically. The regime of the self-induced transparency (where in the presence of the ω-wave the increasing amplitude of the 2ω-wave induces fall in the absorption of the 2ω-wave) is also predicted. These predictions are explained as a manifestation of the nonlinear hysteretic absorption in the case of two-frequencies mixing. The role of the transition from the emission of the simplex wave to the emission of the complex wave (or vice versa) in the process of the induced absorption and transparency is identified.

The article is organized as follows. In Sec. 2 we remind the mathematical formalism of the phenomenological description of nonlinear acoustic wave propagation in mesoscopic materials. In Sec. 3 the numerical integration scheme is presented and tested against the analytical results available for the nonlinear propagation of the initially sinusoidal wave. Section 4 provides the results of the numerical modeling of the simplex and complex waves propagation in the case of the biharmonic initial signal. In Sec. 5, on the basis of the analytical analysis the role of the nonlinear hysteretic absorption in the phenomena under the investigation is revealed. The article is terminated by the discussion (Sec. 6) and the conclusions (Sec. 7).

2. Evolution Equation for Medium with Hysteretic Nonlinearity

We start with the wave equation of propagation of a plain acoustic wave:

$$\rho_0 \left(\frac{\partial^2 u}{\partial t^2} - c_0^2 \frac{\partial^2 u}{\partial x^2} \right) = \frac{\partial \sigma_H}{\partial x} \,,$$

written for the particle displacement u (parallel to the direction of the wave propagation). Here c_0 is the sound velocity, σ_H is a contribution to the stress due to presence of hysteretic elements. So in this model we do not take into account "classical" nonlinearity, concentrating on hysteretic nonlinearity only.[20–22]

Using the well-known method of a slowly varying wave profile (multiple scale technique) described, for example, in Ref. 24, we arrive to the "shortened" (evolution) equation for slowly varying profile of strain $s \approx \partial u/\partial x$ in the wave propagating in the positive direction

of x-axis

$$\frac{\partial s}{\partial x} + v\,(x,\tau)\,\frac{\partial s}{\partial \tau} = 0\,. \tag{2.1}$$

Here $\tau = t - x/c_0$ denotes the "fast" retarded time, x is the "slow" evolution coordinate, and

$$v(x,\tau) = -\frac{1}{2\rho_0 c_0^3}\frac{\partial \sigma_H}{\partial s}\,. \tag{2.2}$$

Equation (2.1) in partial derivatives is known to be equivalent to a system of two ordinary differential equations[24–26]: $ds/dx = 0,\ d\tau/dx = v$. Consequently from the physics point of view the function $v(x,\tau)$ describes the time shift $d\tau$ of a point of the wave profile in the accompanying coordinate system with increasing propagation distance $d\tau = vdx$. Although $v(x,\tau)$ has the dimension of the inverse velocity we will, following the tradition,[26] call it the "velocity" of the wave profile point on the plane (s,τ). In fact it is possible just from the beginning to choose instead of the slow coordinate x a slow time $t = x/c_0$ simultaneously using a fast coordinate $\xi = x - c_0 t = -c_0\tau$ instead of the fast time.[26] Then Eq. (2.1) transforms into $\partial s/\partial t - c_0^2 v\partial s/\partial \xi = 0$ and the coefficient in front of the second term has not only a sense of velocity, but also the dimension of the velocity. However here we prefer to analyze wave evolution as a function of the propagation distance and not of the propagation time (although the two descriptions are directly related) but keeping the term "velocity" for $v(x,\tau)$. Please note that, surely, it is also possible to use in the multiple scale approach for the derivation of the evolution equation both (slow and fast) variables with the same dimension of length (or time). The differences between all possible forms of evolution equation can be eliminated by a suitable choice of the normalized nondimensional variables.

In accordance with Eq. (2.2) the velocity $v(x,\tau)$ is directly proportional to the derivative $\partial\sigma_H/\partial s$ of the stress–strain relationship $\sigma_H(s)$. Consequently one should add an equation of state (i.e. stress–strain relationship) in order to complete the model. Following the ideas of the Preisach–Mayergoyz space formalism we assume here that the nonlinear contribution to stress can be represented by a linear superposition of the contributions σ_{M} from individual mesoscopic hysteretic mechanical elements:

$$\sigma_H(s(x,\tau)) = \sum_{\mathrm{M}\in x} \sigma_{\mathrm{M}}\,. \tag{2.3}$$

Here subscript M marks mechanical elements in the elementary volume at a coordinate x. For the application of the continuous elasticity theory to the analysis of the wave propagation stress should be locally defined in each elementary volume (point) with the dimensions much less than the acoustic wavelength. At the same time it is assumed that an elementary volume contains a huge number of the hysteretic mechanical elements with the dimensions significantly exceeding inter-atomic length scale (mesoscopic elements).

Equation (2.3) formally corresponds to the action of the noninteracting mechanical elements in the elementary volume in parallel (summation of forces). The derivation of the stress/strain relationship for the mesoscopic material can also be achieved starting from the

statement that the change of the elementary volume in the material is a result of a linear superposition of the volume changes exhibited by the individual mechanical elements.[15] The latter statement formally corresponds to the action of the noninteracting mechanical elements in the elementary volume in sequence (summation of the displacements). Using Eq. (2.3) and the strain–strain PM-space we derive (as it is demonstrated in Ref. 21 and later here) the nonlinear dependence of stress on strain, while the summation of the volume changes implies the utilization of the stress-stress PM-space[15] and leads to the dependence of strain on stress. The latter should be inverted to get the dependence of stress on strain required by Eq. (2.2). Importantly in the framework of the nonlinear acoustics these two approaches provide the equivalent results.

It is worth reminding here that nonlinear acoustics by its definition investigates waves with low acoustic Mach numbers. In nonlinear acoustics the deviation $f_{NL}(\sigma)$ of the strain/stress relationship $s(\sigma)$ from the Hooke's law is always small: $s = \sigma/E + f_{NL}(\sigma)$, $|f_{NL}(\sigma)| \ll |\sigma/E|$. Here σ and E denote the stress and the elastic modulus, respectively. Due to $|f_{NL}(\sigma)| \ll |\sigma/E|$, in order to transform $s(\sigma)$ relationship into $\sigma(s)$ relationship (which is more convenient for deriving the acoustic wave equation) it is sufficient to use the Hooke's law approximation $s \cong \sigma/E$ for the inversion of the nonlinear term[12]:

$$\sigma \cong E[s - f_{NL}(Es)] .$$

It is important that the functional form of the nonlinear terms in both $s(\sigma)$ and $\sigma(s)$ relationships is the same in nonlinear acoustics. As a consequence for nonlinear acoustics there is no difference which one of the PM-spaces with homogeneous distribution of the elements (i.e. stress-stress or strain-strain) is used for the modeling of the hysteretic nonlinearity. For the direct modeling of the strain/stress relationship the stress-stress PM-space should be applied. We prefer to use strain-strain PM space because it provides directly the stress/strain relationship for the substitution in the wave equation.[21]

The goal of further consideration is to analyze the typical influence of hysteretic elements on the nonlinear distortion of signal shape. So let us consider the simplest hysteretic function of a rectangular shape for individual mesoscopic element (Fig. 1). Here we note that the hysteretic element used by us here in the strain-strain PM-space transforms (with an accuracy of the second order of smallness) in the hysteretic element used by others in the stress-stress PM-space[15] by applying the Hooke's relation between s and σ (that is via the substitution of σ/E for s and of Es for σ at the axes of Fig. 1). This once again ensures the equivalency of the two approaches in the framework of the nonlinear acoustics.

The introduction of the model element means that we have turned from study of a complicated system consisting of multiple microscopic cracks (or defects) to the consideration of fictional elements, that can be found in one of two states: "open" or "closed" (one denotes these states as $\mathrm{S}(\mathsf{M}) =$"O" and $\mathrm{S}(\mathsf{M}) =$ "C", respectively). The parameters of such an element are just $\sigma_c, \sigma_o, s_c, s_o$. Here s_o is a value of strain at which the element opens while we increase s, and s_c is a value needed to close it if strain decreases ($s_c < s_o$). We also admit instantaneous switching.

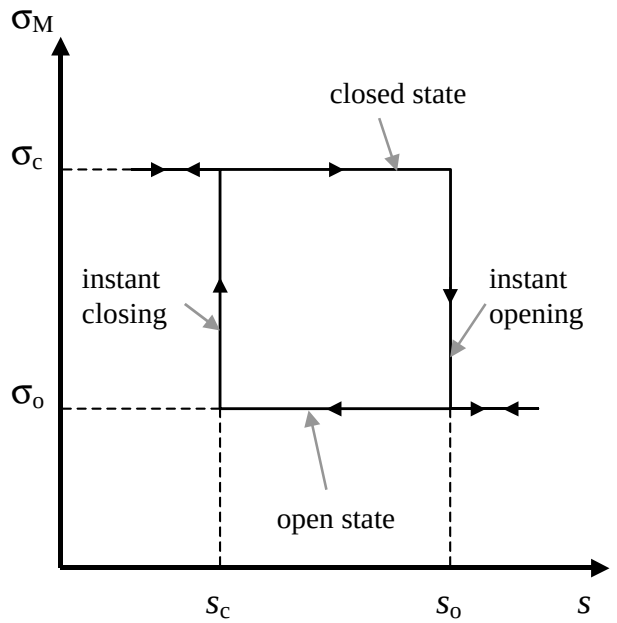

Fig. 1. A hysteretic model of an individual mesoscopic element M. The element is parameterized by values of s_o, s_c, and $\Delta\sigma = \sigma_c - \sigma_o$.

In order to evaluate the derivative $\partial\sigma_H/\partial s = \sum_{\mathrm{M}\in x} \partial\sigma_{\mathrm{M}}/\partial s$ one needs to differentiate the curve plotted in Fig. 1:

$$\frac{\partial\sigma_{\mathrm{M}}}{\partial s} = \Delta\sigma\,\Theta\left(s, s_o, s_c, \mathrm{sign}\left(\frac{\partial s}{\partial\tau}\right), \mathrm{S(M)}\right), \qquad \Delta\sigma = \sigma_c - \sigma_o > 0\,,$$

where

$$\Theta\left(s, s_o, s_c, \mathrm{sign}\left(\frac{\partial s}{\partial\tau}\right), \mathrm{S(M)}\right) = -\begin{cases} \delta(s-s_o), & \text{if } \mathrm{S(M)} = \text{“}C\text{”},\ \partial s/\partial\tau > 0 \\ \delta(s-s_c), & \text{if } \mathrm{S(M)} = \text{“}O\text{”},\ \partial s/\partial\tau < 0 \\ 0, & \text{if } \mathrm{S(M)} = \text{“}C\text{”},\ \partial s/\partial\tau < 0 \\ 0, & \text{if } \mathrm{S(M)} = \text{“}O\text{”},\ \partial s/\partial\tau > 0 \end{cases}, \tag{2.4}$$

and then calculate the velocity in Eq. (2.2). Note that at each value of strain after calculation of the derivative given by Eq. (2.4) we must keep track of the state S(M), reassigning S(M) = “O” in the first case in Eq. (2.4) (with $\delta(s-s_o)$) and S(M) = “C” in the second case (with $\delta(s-s_c)$). In other words, the state S(M) of an element M depends not only on the current value of strain but also on the strain rate:

$$\mathrm{S(M)} = \begin{cases} \text{“}O\text{”}, & \text{if } s_o \le s \\ \text{“}O\text{”}, & \text{if } s_c \le s \le s_o,\ \partial s/\partial\tau < 0 \\ \text{“}C\text{”}, & \text{if } s \le s_c \\ \text{“}C\text{”}, & \text{if } s_c \le s \le s_o,\ \partial s/\partial\tau > 0 \end{cases}, \tag{2.5}$$

as it is illustrated in Fig. 1. Here one should stress the principal feature of the system under study: only the elements changing their state under a current s contribute to stress variation. This is easy to understand if we note that a nonzero derivative in Eq. (2.4) can be found only in cases with delta functions, when according to Eq. (2.5) the state change to the opposite one.

Then for simplicity one considers $\Delta\sigma = \sigma_p - \sigma_o$ for all the elements to be equal and independent of x, and parameters s_o and s_c to be uniformly distributed in the triangle $\Delta = \{(s_o, s_c)\colon -\bar{s} < s_o < \bar{s},\ -\bar{s} < s_c < s_o\}$. This means that the distribution function $f(s_o, s_c) = f_0 = \text{const}$. (here $f(s_o, s_c)ds_o ds_c$ is the number of mechanical elements in the PM-rectangle $(s_o, s_o + ds_o) \times (s_c, s_c + ds_c)$). Certainly for further numerical analysis these assumptions are not that important: we could consider two nontrivial distributions $f(s_o, s_c)$ and $f_\sigma(\Delta\sigma)$ (if $\Delta\sigma$ for all the elements are not equal) both dependent on x, if necessary. Note that despite of the use of the simplest distributions for $\Delta\sigma$ and (s_o, s_c), the parameter $\bar{s}$ (related to the size of PM-triangle containing mechanical elements) is still left arbitrary. It must be, however, larger than amplitude of strain oscillations.

Making use of the above simplifications and changing the summation in Eq. (2.3) for integration, one writes:

$$\begin{aligned}\frac{\partial\sigma_H}{\partial s} &= \int_{-\infty}^{+\infty} ds_c \int_{-\infty}^{+\infty} ds_o \frac{\partial\sigma_{\mathsf{M}}}{\partial s} f(s_o, s_c) \\ &= f_0\Delta\sigma \int_{-\bar{s}}^{s_o} ds_c \int_{s_c}^{\bar{s}} ds_o \Theta\left(s, s_o, s_c, \operatorname{sign}\left(\frac{\partial s}{\partial\tau}\right), \mathrm{S}(\mathsf{M})\right). \end{aligned} \tag{2.6}$$

The Eqs. (2.1), (2.2), (2.4) and (2.6) become a complete set of equations describing the strain wave propagating in a material with hysteretic mesoscopic elements.

We also have to add the boundary condition:

$$s(x = 0,\ \tau) = s_b(\tau) \tag{2.7}$$

and the initial condition for the state of the elements

$$\mathrm{S}(\mathsf{M})|_{\tau=0} = \mathrm{S}_0(\mathsf{M})\,, \tag{2.8}$$

that can, in general, depend on x.

For graphical illustration of mesoscopic elements switching we have plotted Fig. 2(a), that contains a series of pictures in PM-space, corresponding to different points (0–15) of the strain curve $s(\tau)$ in Fig. 2(b). The strain evolution presented in Fig. 2(b) is chosen rather arbitrary.

If a given point s is located on the part of the wave profile with a positive value of the strain rate, then all elements at the left of a vertical line $s_o = s$ in PM-space are open. This line moves to the right as the strain $s(\tau)$ increases, switching all closed elements it is passing through. After reaching strain maximum the "switching line" becomes horizontal ($s_c = s$), it moves down, closing the elements over it. This process continues until a minimum of $s(\tau)$ is achieved, and then turns again to opening (by the vertical line $s_o = s$). Thus the

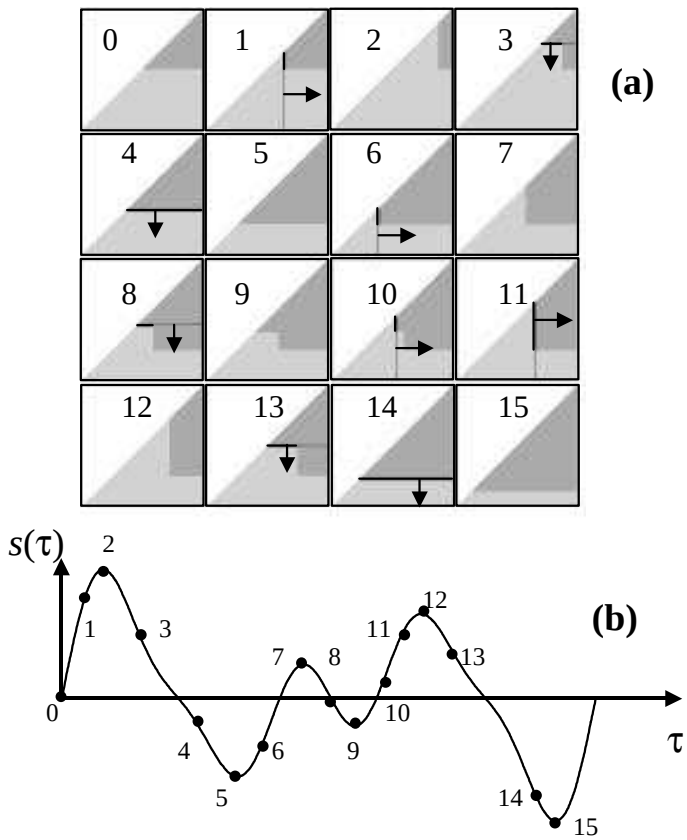

Fig. 2. Illustration of switching in PM-space. The pictures 0–15 (a) are patterns in (s_o, s_c)-PM-space corresponding to the points on the strain curve $s(\tau)$ below (b). The arrows indicate the direction of switching. Areas containing open elements are plotted in light gray, areas containing the closed ones are dark gray. The "switching lines" are marked by thin lines in each portrait, the "switching sections" are thicker. The pictures 2, 5, 7, 9, 12, 15 correspond to the end points (local extrema of $s(\tau)$).

distribution of open and closed elements at any moment of time τ depends on extrema of strain curve in preceding moments. However, the system does not "remember" all the extrema achieved in the past. During the evolution the tracking on some of them is lost. For example, the states 8–10 in Fig. 2 contain the information on the preceding weak maximum 7, but passing to the state 11 erases the memory about it.

Now let us examine the evolution of the velocity $v(x,\tau) = -(2\rho_0 c_0^3)^{-1}\partial\sigma_H/\partial s$ (Eq. (2.2)), that describes deformation of strain profile and is a key point of all our constructions. First imagine that all elements located to the right of the "opening" line $s_o = s$ were initially closed. Then Θ in Eq. (2.4) equals to $\delta(s - s_o)$, and Eq. (2.6) gives[21]:

$$\frac{\partial\sigma_H}{\partial s} = -f_0\Delta\sigma\int_{-\bar{s}}^{s_o} ds_c \int_{s_c}^{\bar{s}} ds_o\delta(s - s_o) = -f_0\Delta\sigma\int_{-\bar{s}}^{s} ds_c = -f_0\Delta\sigma(s + \bar{s})\,, \qquad (2.9)$$

that is, in fact, just the length of this line (multiplied by $f_0\Delta\sigma$). In the case of closing the

situation is similar:

$$\frac{\partial \sigma_H}{\partial s} = -f_0 \Delta\sigma \int_{-\bar{s}}^{s_o} ds_c \int_{s_c}^{\bar{s}} ds_o \delta(s - s_c) = -f_0 \Delta\sigma \int_{s}^{\bar{s}} ds_o = -f_0 \Delta\sigma (\bar{s} - s)\,. \qquad (2.10)$$

Now, if we take into account that in reality not all the elements of the line are switched (i.e. some of them are in the same state before and after the passage of the switching line), we conclude that $\bar{s} \pm s$ in the above equations has to be replaced by the section of the switching line providing the boundary between open and closed areas in PM-space. In all PM-patterns of Fig. 2 such "switching sections" are marked by thicker lines. This is just another (graphical) interpretation of the Eqs. (2.4)–(2.6) showing that only the elements changing their state at a given τ will give a contribution to the nonlinearity.

So, generally speaking, the process of strain wave propagation in a medium with hysteretic elements has the memory about its history, namely about some of strain extrema. Thus, unfortunately, further analytical consideration encounters serious difficulties, since one has to keep track on the state $\mathsf{S}(\mathsf{M})$ of mesoscopic elements, solving the system of Eqs. (2.1), (2.2), (2.4)–(2.8), that contains both continuous and discrete functions.

Such statement of the problem is rather complete, but it has a serious disadvantage: the solution will depend on some arbitrary parameters, as the initial configuration of open and closed areas in PM-space (in a real experimental situation we do not know it in advance), together with the outer limit of PM-triangle. However, if we consider a periodical signal, then after passing one period this configuration will be erased. Of course, the second period will still carry some information on the initial state, since the first one when erasing the initial state was additionally distorted. But the subsequent periods will contain this information in lesser and lesser degree. In other words, we expect that after passing a large number of cycles the process will converge to a stationary one. This means that the acoustic wave "prepares" the medium for itself.[22] This stationary solution in the "prepared" medium is a goal of our consideration.

Let us compare the method proposed above and the numerical simulation LISA (local interaction simulation approach), reported in a cycle or papers by M. Scalerandi, P. P. Delsanto *et al.* (see, for example, Refs. 27 and 28). The latter also assumes 1D geometry and PM-distribution of hysteretic units and produces quite similar results in the case of the sinusoidal input (in particular, odd-order harmonics dominance in the spectrum). However, instead of a continuous medium LISA considers a discrete system (a chain) of mechanical elements, which can be elastic and/or hysteretic. An element at a coordinate x corresponds to a point in PM-space, whereas in the description above one x-point corresponds to a whole PM-space, since the summation (Eq. (2.3)) is applied over all hysteretic units belonging to a physically small volume. As soon as a model for the hysteretic elements is chosen and the statistical distribution of their parameters is known both approaches should provide equivalent results for long acoustic waves. We perform analytically the averaging (homogenization) of the material properties, while LISA does this in the process of numerical computing. This difference is demonstrated by results[27,28] obtained by LISA, which are affected by uncertainty coming from the fact that each x-point has random (and not averaged) hysteretic

properties. In our opinion, the major advantage of LISA is in its future possible application to the analysis of short waves propagation, where there are just a few different hysteretic elements at the scale of the acoustic wavelength and the homogenization is not possible.

3. Numerical Solution of the Evolution Equation

3.1. *Numerical integration scheme*

Now let us turn to the numerical procedure we have developed for realization of the aforementioned goal. First we introduce dimensionless variables, assuming a periodic strain wave at the boundary ($x = 0$) with a period τ^0 and characteristic strain value s^0. These variables are:

$$\tau' = \frac{\tau}{\tau^0},\ s' = \frac{s}{s^0},\ x' = \frac{x}{x_{nl}},\ v' = v\frac{\tau^0}{x_{nl}},\ c_0' = c_0\frac{\tau^0}{x_{nl}} \tag{3.1}$$

where

$$x_{nl} = \frac{2\tau^0\rho_0 c_0^3}{\Delta\sigma f_0 s^0} \tag{3.2}$$

is a characteristic length of the nonlinear interaction.[20–22] Below in the text the primes are omitted.

Methods of solving the transport equation (Eq. (2.1)) are well known. We have used a symmetrical scheme with centered finite differences given by:

$$\frac{1}{2\Delta x}(s_j^{i+1} - s_j^i) + \frac{1}{2\Delta x}(s_{j+1}^{i+1} - s_{j+1}^i) + \frac{v}{2\Delta\tau}(s_{j+1}^i - s_j^i) + \frac{v}{2\Delta\tau}(s_{j+1}^{i+1} - s_j^{i+1}) = 0\,. \tag{3.3}$$

Here $s_j^i = s(x_i, \tau_j),\ i = 1, \ldots, N_x,\ j = 1, \ldots, N_\tau$, is the discrete strain function, defined on the grid $x_i = \Delta x(i-1)$, $\tau_j = \Delta\tau(j-1)$ where the steps $\Delta x = X/(N_x - 1)$, $\Delta\tau = T/(N_\tau - 1)$ and X and T are intervals of consideration for space and time, respectively (all variables are dimensionless).

This scheme has the second order of approximation and requires the common stability conditions:

$$v_{\max}\Delta x < \Delta\tau\,, \tag{3.4}$$

but in order to run it we need some additional information about strain values at the next x-layer $i + 1$. Here we have two possibilities as following:

(i) The most direct way is to start with the state depicted in Fig. 2(0), where all elements with $s_c > 0$ are closed and the elements $s_c < 0$ are open (or any other similar distribution containing initially open and initially closed elements). In addition we also have to consider a signal on entry (the boundary condition $s_b(\tau)$) starting with increasing front and having $s_b(0) = 0$. Such a configuration on open and closed areas will lead to the velocity v to be 0 at the first moment of time. Indeed, the switching section AB in Fig. 2(1) has zero length at the moment $\tau = 0$. This means that the first point ($\tau = 0$) of the strain profile will never

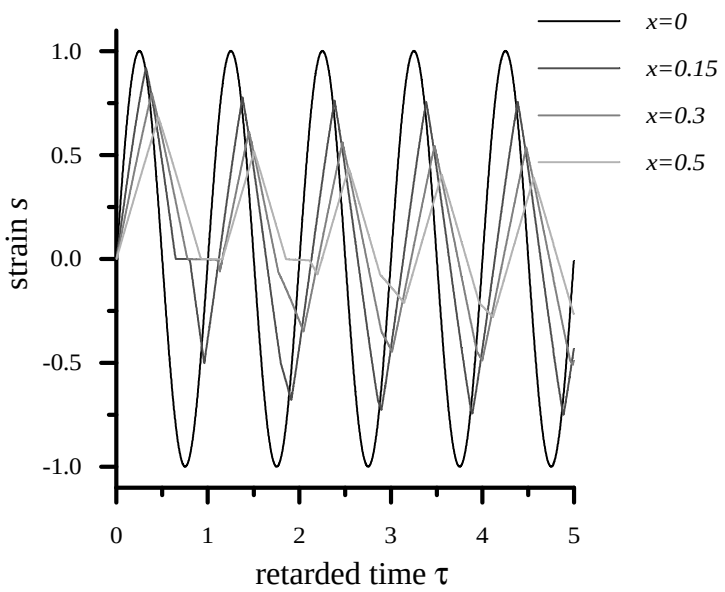

Fig. 3. Illustration of the transition process: the nonlinear distortion of a strain sinewave $s(x=0,\tau) = \sin 2\pi\tau$, calculated for different depths x. The outer limit of PM-space: $\bar{s}=2$.

be shifted and we can fix $s(x,0)=0$, i.e. $s_1^i = 0$ for each point x_i. Then, having $s_j^1 = s_b(\tau_j)$ at $x=0$, $s_1^i = 0$ at $\tau = 0$, we calculate s_{j+1}^{i+1} from known values of $s_j^i, s_{j+1}^i, s_j^{i+1}$:

$$s_{j+1}^{i+1} = F(s_j^i, s_{j+1}^i, s_j^{i+1})\,, \tag{3.5}$$

where function F can be easily found by resolving Eq. (3.3) with respect to s_{j+1}^{i+1}.

This scheme is valid if the velocity of the strain profile's translation $v \geq 0$ for every number i and j, because only in this case the profile shifts entirely in the positive direction, so that all s_1^i are retained undistorted (and equal to 0). Note that this condition is obviously fulfilled (see Eqs. (2.2) and (2.4)).

The main disadvantage of such an approach is that we have in this case a long transient process before achieving the stationary solution. For instance, the starting point of the first period of the strain curve is unmovable, but the starting points of all other cycles will be shifted, because at these points we have nonzero value of v. Running ahead, we plotted in Fig. 3 such transitional process, when the stationary strain profile is greatly distorted by the influence of the initial condition.

Therefore we preferred another method consisting of computing the stationary profile itself as described below.

(ii) For periodic excitation, let us consider periodic conditions for each strain curve against time. This means that one defines additional $(N_\tau + 1)$th point of the time discretization, assuming $s_{N_\tau+1}^i = s_1^i$ and the same step $s_{N_\tau+1}^i - s_{N_\tau}^i = \Delta\tau$ $(i = 1, \ldots, N_x)$. Then we have a complete system of equations for a new x-layer $i+1$. To solve it, we have used iterative method as following: define an iteration sequence $\tilde{s}_j^{(k)}$ for the kth iteration

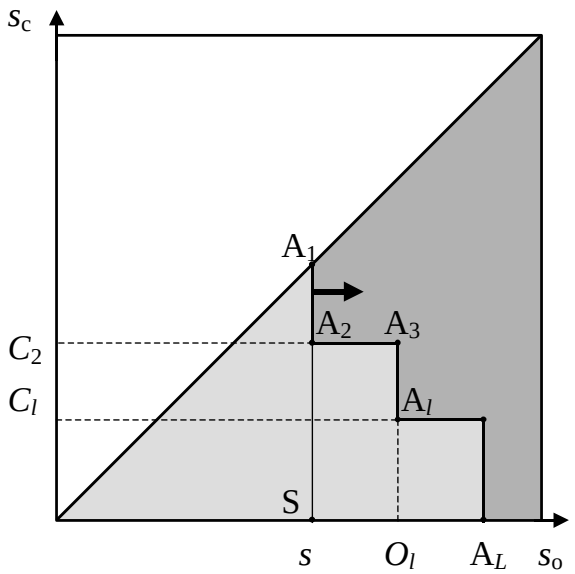

Fig. 4. The parametrization of PM-space configuration by the corner points $A_1, A_2, \ldots, A_l, \ldots, A_L$ of the boundary between open (light gray) and closed (dark gray) areas. The "switching line" is A_1S, the "switching section" is A_1A_2.

and $(i+1)$th x-layer, admit $\tilde{s}_1^{(1)} = s_1^i$, then compute $\tilde{s}_{j+1}^{(1)} = F(s_j^i, s_{j+1}^i, \tilde{s}_j^{(1)})$ in order to have $\tilde{s}_{N_\tau+1}^{(1)}$, then use the periodical condition and fix $\tilde{s}_1^{(2)} = \tilde{s}_{N_\tau+1}^{(1)}$, etc. Calculations show that the second iteration is already sufficient to achieve the equality $s_{N_\tau+1}^{i+1} = s_1^{i+1}$.

However, this is still not enough to run the numerical scheme. To calculate the strain profile at the next x-step $i+1$ we also need to know the configuration of open and closed areas in PM-space in the beginning of each period. Otherwise it is impossible to obtain the value v that is presented in Eq. (3.3). To fix such a configuration we use the following fact: for a periodical signal one can start moving to the next x-layer $i+1$ according to Eq. (3.4), taking any arbitrary τ-index $j = j_1$ as initial and substituting the points with lesser numbers j to the end of the strain curve. That is, we redefine the strain profile as:

$$\hat{s}_{j-j_1+1}^i = s_j^i \text{ for } j_1 \le j \le N_\tau, \qquad \hat{s}_{N_\tau+j-j_1+1}^i = s_j^i \text{ for } 1 \le j \le j_1 - 1\,, \tag{3.6}$$

and then use Eq. (3.5) to obtain the sequence $\hat{s}_j^{i+1},\ j = 1, \ldots, N_\tau$. Now, if we take j_1 at the point of global maximum $s_{j_1}^i = s_{\max}$ of the strain s_j^i at the current x-layer, the corresponding PM-pattern is known: all elements are open. In this manner, we start calculations for the shift to the global maximum strain profile first using Eq. (3.5) and then performing the back substitution $\hat{s}_j^i \to s_j^i$ according to Eq. (3.6). The hats in the denotations will be omitted for brevity.

The stability condition (Eq. (3.4)) for a stationary solution takes the form: $(s_{\max} - s_{\min})\Delta x < \Delta$ since the maximum v does not exceed the maximum strain peak-to-peak amplitude.

This method was chosen for performing all further computations, because it yields strictly periodical (i.e. stationary) solution without having a need to consider many periods in order to reach the convergence. Thus we found an appropriate algorithm to obtain v without time-consuming direct consideration of transient processes.

3.2. *Calculation of the nonlinear coefficients of the numerical scheme*

The numerical scheme based on Eq. (3.3) has a nonlinear coefficient — the velocity v of strain profile's deformation, or, in other words, the derivative $\partial\sigma/\partial s$ of the stress–strain relationship (Eq. (2.2)). First of all, in order to proceed from ith x-layer to $(i+1)$th, the only possibility we have is to take all nonlinear coefficients at ith layer, where all variables are known. In the dimensionless variables this velocity is given by the expression:

$$v(x_i, \tau_j) = \int_{-\bar{s}}^{s_o} ds_c \int_{s_c}^{\bar{s}} ds_o \Theta\left(s, s_o, s_c, \operatorname{sign}\left(\frac{\partial s}{\partial \tau}\right), \mathrm{S}(\mathsf{M})\right) . \tag{3.7}$$

The r.h.s. of this equation, as it was demonstrated above, corresponds to the length of the section of the boundary between open and closed sectors in PM-space determined by the straight lines $s_o = s$ or $s_c = s$ (see Fig. 2). Since the chosen scheme is symmetrical, it is reasonable to substitute s here by $1/2(s_j^i + s_{j+1}^i)$ to keep the order of approximation.

To calculate numerically the length of the switching section one needs first to parameterize a configuration of open and closed areas of PM-space. As the orientation of the switching section is always vertical or horizontal, and it opens all elements at the left of it (if it is vertical) and closes all elements above it (if it is horizontal), any arbitrary complicated pattern always consists of two areas (one fully open and one fully closed) and a staircase (stepwise) boundary between them.[17,18] Such a boundary is represented by the broken line $A_1A_2, \ldots, A_l, \ldots, A_L$ in Fig. 4. So, any possible configuration of PM-space under acoustical excitation is completely described by the coordinates of these end-points, which we denote as $A_l = (O_l, C_l)$, $l = 1, \ldots, L$ (see Fig. 4). The point A_1 lays on the diagonal and has the coordinates (s, s), all the other corner points are to be kept in memory. After such parameterization, in order to obtain the velocity v (the length of the section A_1A_2) on a given x-layer for every τ-point, one needs to shift the points A_1 and A_2 in accordance with temporal strain variations $s(\tau)$, erasing the points A_2 and A_3 if at one moment they coincide, and creating a new A_1-point on the diagonal, if one of the extrema of $s(\tau)$ is reached. This procedure in details looks like the following.

First, on a fixed x_i-layer we find the global extrema $s_{\max}$ and $s_{\min}$ of s_j (superscript i is omitted) and then shift the strain profile according to Eq. (3.6) in order to begin with the global maximum. At that position we take fully open PM-space, defining A_1A_2 section at the left boundary of PM-space: $A_1 = (s_{\max}, s_{\max})$, $A_2 = (s_{\max}, s_{\min})$, and start cycles $j \to j{+}1$. In each cycle we analyze whether the current strain value s_{j+1} belongs to an increasing or decreasing front of the strain profile (just comparing s_j and s_{j+1}). Considering now for definiteness an increasing front (opening), we reassign the coordinates O_1 and O_2 of the first two corner points to the value $s = (s_j + s_{j+1}.)/2$ (See Fig. 4) If the new coordinates O_1 and O_2 exceed the value O_3, the memory about the 2nd and the 3rd points should be

erased; we delete these points and renumerate the arrays O_l and C_l so that the former 4th point becomes the 2nd, 5th becomes 3rd, etc.

If the current strain value s_{j+1} is located in the very beginning of the increasing front (i.e. s_j was a local minimum over j) we have to introduce a new point A_1, shifting the indices of all old points by +1. In this way we keep tracking of all local extrema until they are exceeded by larger excursions of strain.

After having the first two points shifted (and, if necessary, renumbering the points) we take the searched nonlinear velocity to be equal to $v = (s^i_j + s^i_{j+1})/2 - C_2$. In the case of a decreasing slope of the strain curve the procedure is analogous, and the velocity $v = O_2 - (s^i_j + s^i_{j+1})/2$. In this way we repeat the procedure until $j = N_\tau$ and then proceed to the next x-layer according to Eq. (3.5).

The proposed algorithm appears to be an exact solution of finite-difference equation (Eq. (3.3)), that is the second order of approximation of the initial differential Eq. (2.1). Keeping track of the state of mesoscopic elements and searching for a stationary solution, we did not use any additional assumptions.

3.3. *Testing the numerical scheme*

In order to examine the precision provided by the discussed method we have used the analytical solution for the dimensionless equation:

$$\frac{\partial s}{\partial x} + \left[s_{\max}(x) + \operatorname{sign}\left(\frac{\partial s}{\partial \tau}\right) s \right] \frac{\partial s}{\partial \tau} = 0, \;\; s(x=0,\tau) = \sin 2\pi\tau$$

that describes the strain wave propagation for the harmonic excitation. This solution in the implicit form[20]:

$$s(x,\tau) = \sin\left[\tau - \int_0^x s_{\max}(\xi) d\xi - \operatorname{sign}\left(\frac{\partial s}{\partial \tau}\right) sx \right] ,$$

is a transcendental algebraic equation. Here $s_{\max}(x)$ is the depth dependence of maximum of $s(x,\tau)$, that is also an unknown function, that results in the profile's shift during the propagation:

$$\tau \to \tau - \int_0^x s_{\max}(\xi) d\xi \equiv \theta \, . \tag{3.8}$$

Solving numerically the equation $s(x,\theta) = \sin[\theta - \operatorname{sign}(\partial s/\partial\theta) sx]$ with very high accuracy (just by the conventional bisectional method, taking the middle point of a current interval for the solution and comparing the r.h.s. and l.h.s. of the equation), we found the shifted profile $s(x,\theta)$, estimated its maximum and recovered $s(x,\tau)$. All test computations were performed for the maximal (deepest) $x = X$, the precision for smaller x being better.

The agreement between the strain profiles calculated via the implicit analytical solution Eq. (3.8) and the above described iteration procedure was found within 0.6% for the number of points in the finite-difference scheme Eq. (3.3) $N_x = 10000$, $N_\tau = 8192$, and $T = 1$, $X = 0.5$ (T and X are spatial and time intervals considered). This accuracy is affected

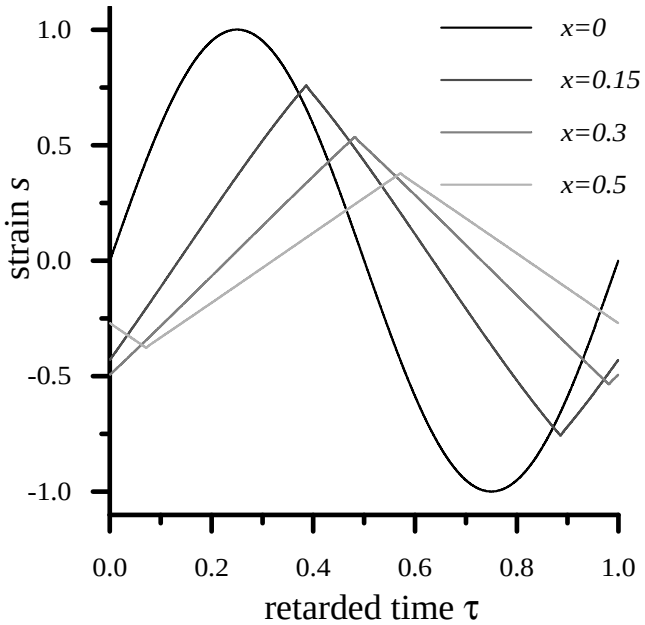

Fig. 5. The nonlinear distortion of a strain wave $s(x=0,\tau)=\sin 2\pi\tau$, calculated at different depths x. The accuracy achieved for $N_x = 10\,000$, $N_\tau = 8192$, $T = 1$ and $X = 0.5$ is 0.6%.

mainly by an uncertainty of the extrema positions, since they play a key role in constructing the solution, but are defined with a lower order accuracy (the 1st order in $\Delta\tau$). Further, since a maximum of a strain profile has the uncertainty of $\Delta\tau$, the cumulative effect for the deepest N_xth profile can be roughly estimated as $\Delta\tau\sqrt{N_x}$ (in our case we had actually the uncertainty values about $10\Delta\tau = 0.0012$ of a period). It was checked that, varying the τ-shift of the iterated profile as a whole and matching it to the exact solution, one has much better accuracy of about 0.01%. We hope that for most applications such a small shift is not important, since it will not influence the strain spectrum, which is of the main interest. Otherwise, it is possible to introduce an additional complication of the algorithm, making use of a more accurate approximation for the strain profile near its maximum.

Due to the above mentioned reasons together with the asymmetric approximation of the nonlinearity (corresponding to the ith layer, but not to the middle between the ith and the $(i+1)$th layers) the resultant order of approximation for the proposed method is less than 2.

The calculated test strain profiles for the sinusoidal signal are shown in Fig. 5. They exhibit all known features for this case[20]: the nonlinear attenuation (described by $s_{\max}(x)$) the nonlinear decrease of sound velocity, the convergence to a saw-like shape at large depths.

We have also tested the accuracy of the calculation results in terms of the strain harmonics $Z_n(x)$:

$$s(x,\tau) = \sum_{n=0}^{\infty} Z_n(x)\sin(2\pi n\tau + \phi_n(x))\,. \tag{3.9}$$

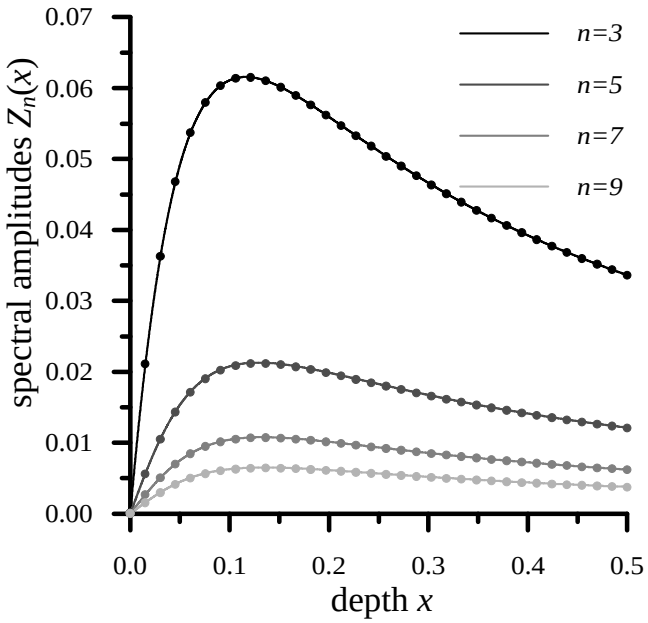

Fig. 6. The generation of the harmonics during the propagation of the single frequency signal: the amplitudes Z_n of harmonics against the depth x. The points indicate the spectral amplitudes Eq. (3.9) for the exact solution Eq. (3.8).

The calculation indicated that for a pure sinusoidal wave $s(x = 0, \tau) = \sin 2\pi\tau$ at the boundary (i.e. $Z_n(0) = \delta_{1,n}$) only odd harmonics are generated, in agreement with Refs. 20, 21 and 23. The depth dependencies of the calculated strain harmonics are shown in Fig. 6 by solid lines, and the harmonics for the exact solution Eq. (3.8) are marked by filled circles. For the chosen numbers of points the precision is found to be 0.03%, 0.46%, 0.47%, and 1.3% for the 3rd, 5th, 7th and 9th harmonics, respectively. As it was expected, this accuracy is much better than one we have for the strain profiles themselves, affected by the uncertainty in the positions of maxima.

4. Numerical Results for Two-Frequency Mixing in Nonlinear Wave Propagation

Using the developed numerical scheme it is possible to analyze the nonlinear propagation of an arbitrary acoustic signal launched from the boundary $x = 0$. However, in order to get an insight in the physics of the process of wave interactions in materials with hysteretic quadratic nonlinearity we present here the results for the signals that are biharmonic at the boundary. Moreover, we limit ourselves to the analysis of a particular case where the signal at the boundary is a mixture of harmonic signals at frequencies ω and 2ω. This particular choice is motivated by the fact that the 2ω-wave is not generated by the ω-wave in materials with hysteretic quadratic nonlinearity (see Fig. 6). This is expected to provide some simplification in the interpretation of the results. More importantly is the fact that

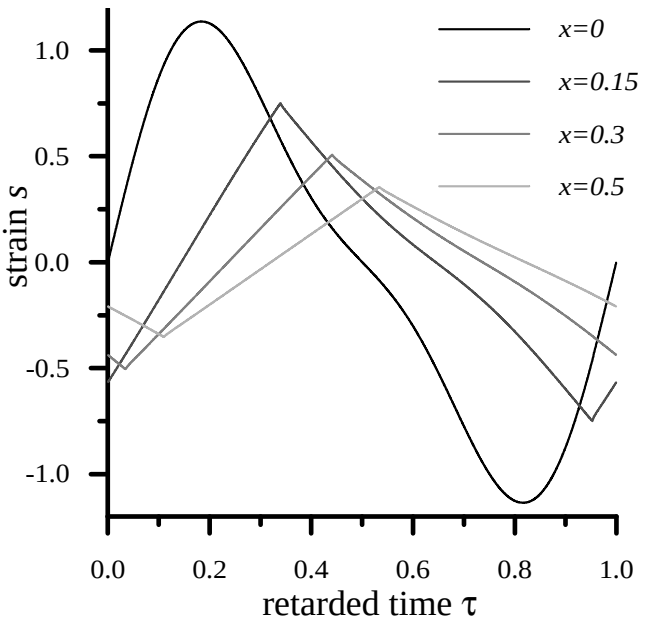

Fig. 7. Nonlinear distortion of the biharmonic strain wave: $s(x=0,\tau) = A_1 \sin 2\pi f_1 \tau + A_2 \sin 2\pi f_2 \tau$. Here $f_1 = 1, f_2 = 2, A_1 = 1, A_2 = 0.2$ ("simplex" profile).

in this case the analytical results describing the nonlinear hysteretic absorption of acoustic waves can be obtained in a limiting regime and can be used both for the additional testing of the numerical scheme and for the interpretation of the numerical results.

In the first set of the simulations we added to the sinusoidal input analyzed in Sec. 3.3 without any phase shift a sinusoidal signal at frequency 2ω. The boundary condition takes the form:

$$s(x=0,\tau) = Z_1(0) \sin 2\pi f_1 \tau + Z_2(0) \sin 2\pi f_2 \tau \equiv A_1 \sin 2\pi\tau + A_2 \sin 4\pi\tau \,. \tag{4.1}$$

Here and in the following we use the notations $A_{1,2}$ for the amplitudes $Z_{1,2}(0)$ of the waves with frequencies ω and 2ω at the boundary. Figure 7 illustrates the nonlinear distortion of the wave profile with increasing propagation distance and Fig. 8 presents the evolution of the spectrum for a typical simplex wave ($A_2/A_1 = 0.2 < 0.5$). Note that for the boundary condition in Eq. (4.1) the complex wave is launched from the boundary if $A_2/A_1 > 0.5$. Figure 9 presents the evolution of the wave profile for a typical complex wave ($A_2/A_1 = 0.7 > 0.5$), while Fig. 10 shows its spectrum. In the spectrum presentations here and later we retain only the frequencies that can be generated by the initial ω and 2ω waves directly by the four-phonon processes. In general in the medium with hysteretic quadratic nonlinearity for frequency mixing of ω_1 and ω_2 resulting in the excitation of ω_3 the following multi-phonon processes are allowed[29,30]: $\omega_3 = \pm(\omega_1) \pm 2m(\omega_2)$ and $\omega_3 = \pm(\omega_2) \pm 2m(\omega_1)$ with arbitrary combination of signs and factors $m = 1, 2, 3, \ldots$. One phonon of frequency $\omega_{1,2}$ and $2m$ phonons of frequency $\omega_{2,1}$ are participating together with the resultant phonon

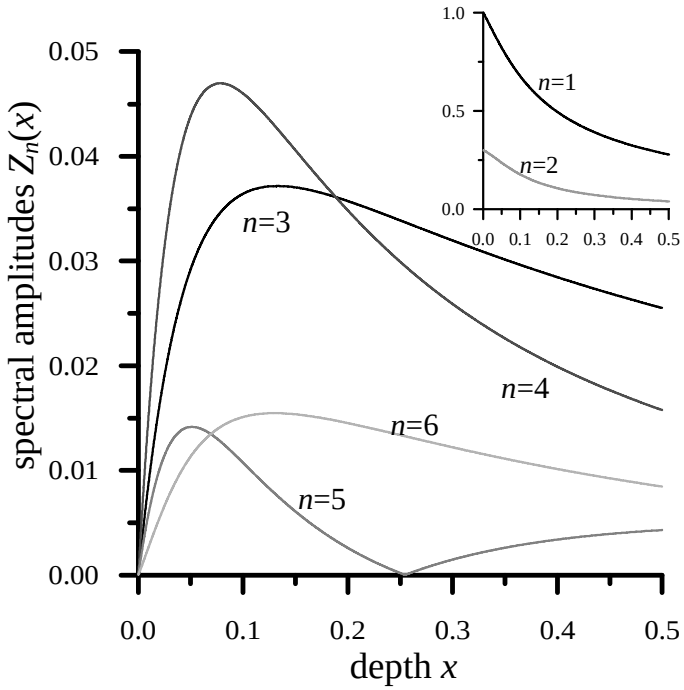

Fig. 8. Generation of higher harmonics during the process of two-frequency wave propagation (Fig. 7): the depth dependences of the spectral amplitudes $Z_n(x)$ for different frequencies $n\omega$.

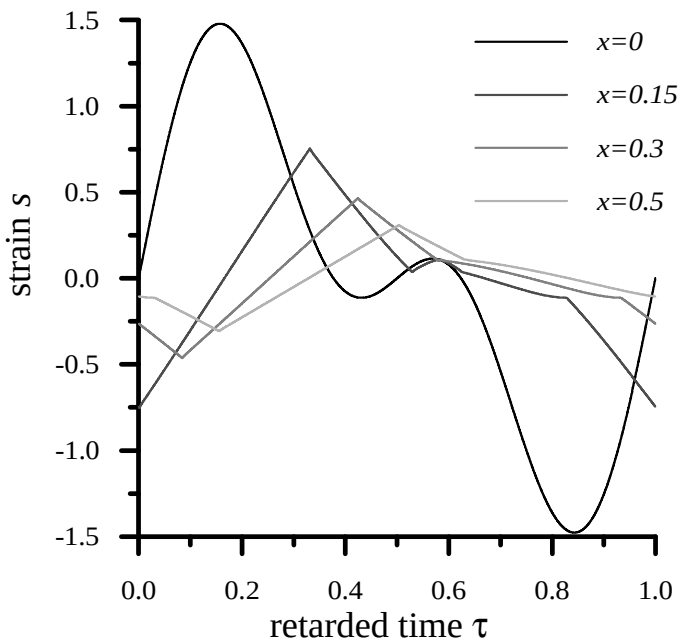

Fig. 9. Nonlinear distortion of the biharmonical strain wave: $s(x=0,\tau) = A_1 \sin 2\pi f_1 \tau + A_2 \sin 2\pi f_2 \tau$. Here $f_1 = 1, f_2 = 2, A_1 = 1, A_2 = 0.7$ ("complex" profile).

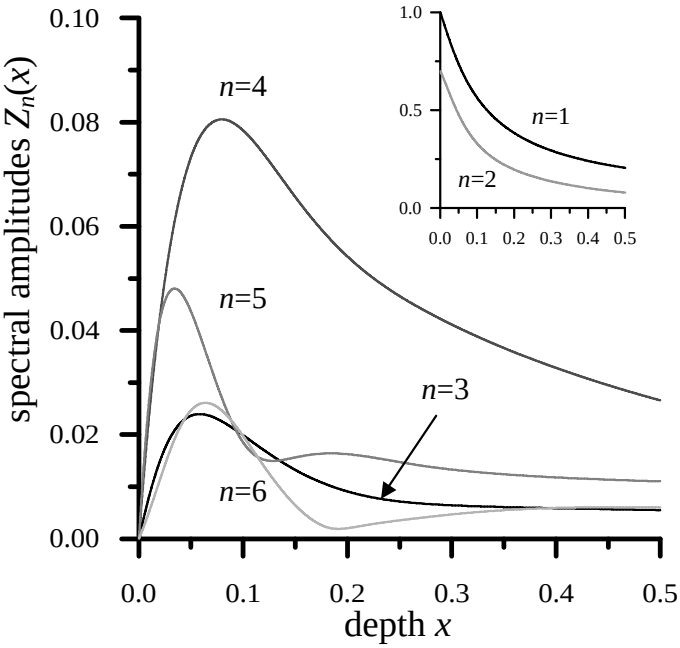

Fig. 10. Generation of higher harmonics during the process of two-frequency wave propagation (Fig. 9): the depth dependences of the spectral amplitudes $Z_n(x)$ for different frequencies $n\omega$.

of frequency ω_3 in each $2(m+1)$-phonon process. However the efficiency of the process diminishes with the increasing m. That is why we keep in our presentation (but, surely, not in the calculations) only the four-phonon processes (corresponding to $m = 1$).

The remarkable feature observed in the spectrum evolution (Figs. 8 and 10) is the faster initial growth of the 4ω-wave in comparison with the 3ω-wave. At first glance this looks unexpectedly because the efficiency of the process $(\omega)+2(\omega) = 3\omega$ (Sec. 3.3) is proportional to A_1^2, while the efficiency of the process of the 4ω-wave generation $(2\omega)+2(\omega) = 4\omega$ (where one phonon of the 2ω-wave is combined with two phonons of the ω-wave) is proportional to A_1A_2, and normally it is lower when $A_2 \ll A_1$ (Fig. 8). However, it should be taken into account that in the presence of the 2ω-wave there is an additional process of the direct excitation of the third harmonic: $-(\omega)+2(2\omega) = 3\omega$, where two phonons of the 2ω-wave are combined with a phonon of the ω-wave. Clearly, the latter process acting in anti-phase to the process $(\omega)+2(\omega) = 3\omega$ could be responsible for the decrease of the 3ω-wave amplitude in the presence of the 2ω-wave (Fig. 8) in comparison with the case of the monochromatic input (Fig. 6). Though this interpretation is plausible, we have in any case to admit that high relative efficiency of the forth harmonic excitation for the particular phasing between the input waves assumed in Eq. (4.1) is amazing.

The important feature extracted from the analysis of the wave profile transformation (Fig. 9) is the gradual transformation of the complex wave into the simplex wave with increasing propagation distance. The local maximum disappears due to the hysteretic absorption, that near the wave extrema has a very clear "geometrical" manifestation. In fact,

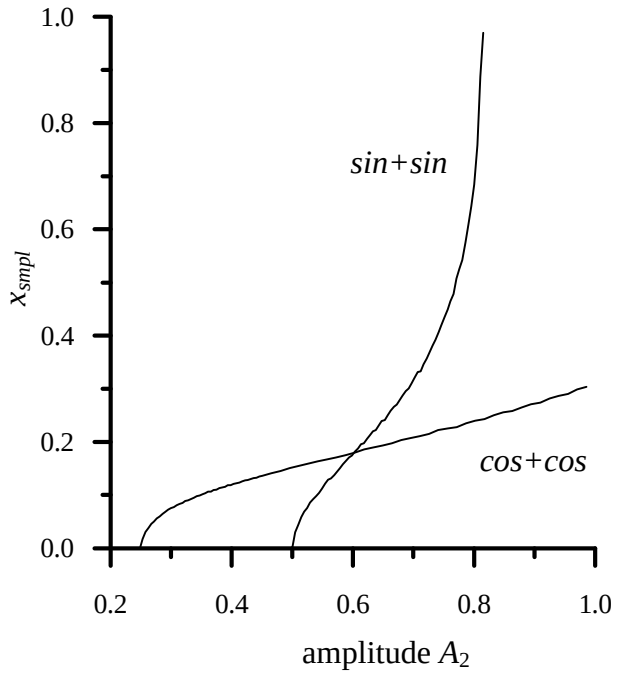

Fig. 11. The critical distance x_{smpl} (the distance when a complex wave becomes simplex) as a function of amplitude A_2 for the boundary conditions Eq. (4.1) ("sin + sin") and Eq. (4.2) ("cos + cos"). Here $A_1 = 1$ in both cases.

similar to the case of a pure sinusoidal wave[20,21] (or to the case of the acoustic pulses[22]) the leading part of the wave profile near the extremum is always delayed due to nonlinear effects relative to the trailing part. An extremum itself is the intersection point of these rising and falling (or vice versa) parts of the profile where the leading part moves near the extremum in the direction of the trailing part.[20]

The formal mathematics demonstrates that the nonlinear contribution to sound velocity is always negative just before the extremum and is equal to zero just after the extremum (see, for example Eq. (5.1) and Eq. (5.4) in Sec. 5). The continuous mutual "penetration" of these leading and trailing parts leads to the diminishing of the strain amplitude in the extremum (compare for example the profiles at $x = 0$ and $x = 0.5$ in Fig. 9). In Fig. 11 we present the dependence of the critical distance x_{smpl} for the end of the transition from the complex to the simplex wave on the amplitude A_2 of the 2ω-wave at the boundary. The proposed numerical algorithm enables us to keep track of the number of extrema directly. From general considerations it might be expected that the frequency mixing processes significantly depend on the relative phase shift between the interacting waves. One of the best-known examples is the dependence of the amplification of the subharmonic $(\omega/2)$ in the field of the ω-wave in material with a classical elastic quadratic nonlinearity on their mutual phasing.[24] For the materials with hysteretic quadratic nonlinearity the dependence of the absorption of a weak probe wave in the field of a strong pump wave on their relative phase was predicted

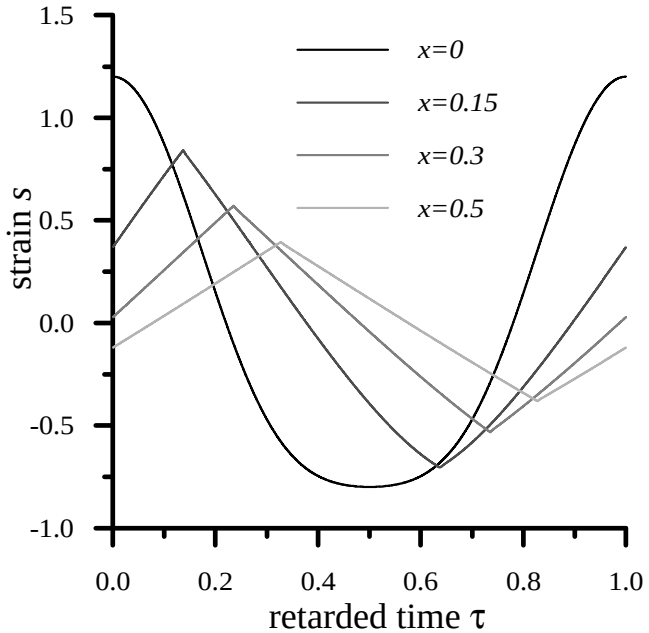

Fig. 12. Nonlinear distortion of the biharmonical strain wave: $s(x=0,\tau) = A_1 \cos 2\pi f_1 \tau + A_2 \cos 2\pi f_2 \tau$. Here $f_1 = 1, f_2 = 2, A_1 = 1, A_2 = 0.2$ ("simplex" profile).

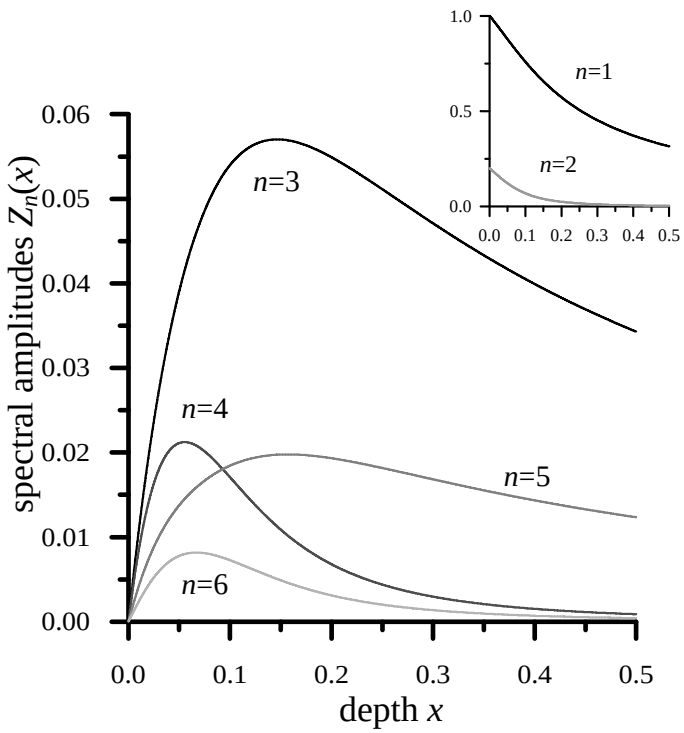

Fig. 13. Generation of higher harmonics during the process of two-frequency wave propagation (Fig. 12): the depth dependencies of the spectral amplitudes $Z_n(x)$ for different frequencies $n\omega$.

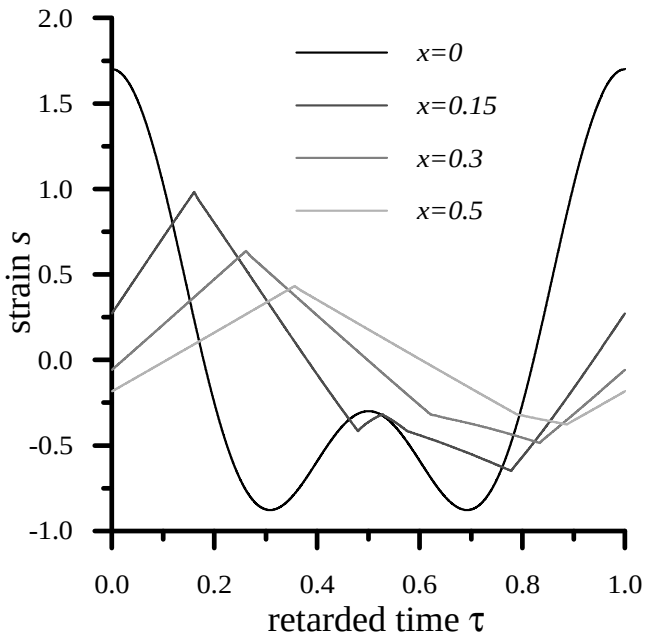

Fig. 14. Nonlinear distortion of the biharmonical strain wave: $s(x=0,\tau) = A_1 \cos 2\pi f_1 \tau + A_2 \cos 2\pi f_2 \tau$. Here $f_1 = 1, f_2 = 2, A_1 = 1, A_2 = 0.7$ ("complex" profile).

theoretically.[31] Following these indications we decided to analyze the case with the boundary condition different from one in Eq. (4.1) and we introduced the shift equal to $\pi/4$ into the 2ω-wave. In fact the possible phase shifts $\Delta\varphi$ leading to qualitatively different results in wave transformation are limited by the interval $0 \leq \Delta\varphi \leq \pi/4$. So the chosen case $\Delta\varphi = \pi/4$ can be considered as the opposite to $\Delta\varphi = 0$ (Eq. (4.1)) limiting case. The boundary condition for $\Delta\varphi = \pi/4$ can be equivalently presented as:

$$s(x=0,\ \tau) = A_1 \cos 2\pi\tau + A_2 \cos 4\pi\tau\,. \tag{4.2}$$

In Figs. 12 and 13 we present for a typical simplex wave the evolution of the profile and the spectrum, respectively. The complex wave exists for the boundary condition Eq. (4.2) if $A_2/A_1 \geq 0.25$. In Figs. 14 and 13 we present for a typical complex wave the evolution of the profile and the spectrum, respectively. The results in Figs. 13 and 15 confirm the hypothesis on the strong dependence of the frequency mixing process in the materials with hysteretic quadratic nonlinearity on the mutual phase of the ω and 2ω waves.

In the case $\Delta\varphi = \pi/4$ the efficiency of the 4ω-wave excitation at short propagation distances does not exceed the efficiency of the third harmonic generation.

In the case of the boundary condition Eq. (4.2) the transformation of a complex wave into a simplex one is also observed (Fig. 14). From Fig. 11 it follows that in this regime (marked as "cos + cos") the simplex wave is formed (for the same ratio A_2/A_1) at shorter propagation distances in comparison with the regime "sin + sin" ($\Delta\varphi = 0$). Qualitatively this is due to higher nonlinear hysteretic absorption near the local extrema in the former

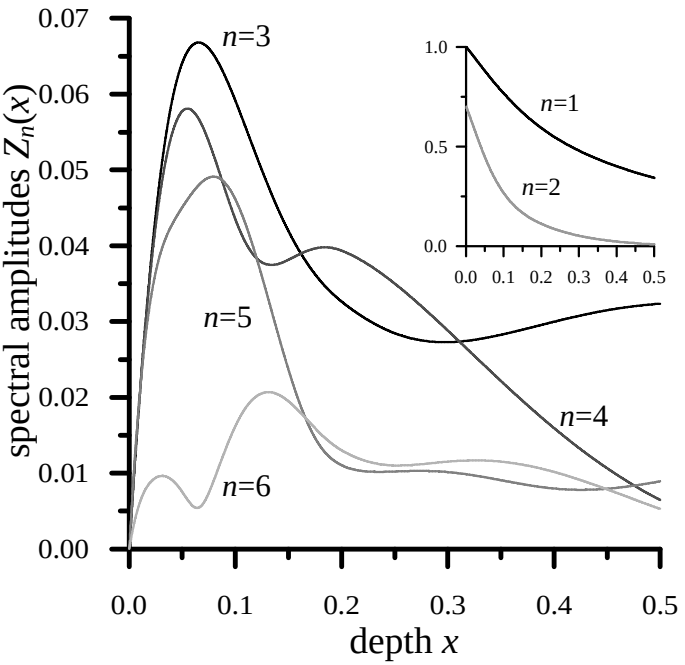

Fig. 15. Generation of higher harmonics during the process of two-frequency wave propagation (Fig. 14): the depth dependencies of the spectral amplitudes $Z_n(x)$ for different frequencies $n\omega$.

regime. In fact the hysteretic absorption in an extremum depends on the magnitude of the differences between the strain value s_e in the considered extremum and the strain s_{ep} in the previous extremum. More precisely the "velocity" of the mutual penetration of the two parts of the wave profile near the extremum is proportional to $|s_e - s_{ep}|$. Comparison of Figs. 9 and 14 clearly demonstrates that at the boundary this factor for the first strain minimum is larger in the regime $\Delta\varphi = \pi/4$ than in the regime $\Delta\varphi = 0$. The larger critical length x_{smpl} in the regime "sin + sin" can be attributed to the fact that in this regime the formation of the internal loop (characteristic to the complex process) leads to nearly twice reduction of $|s_e - s_{ep}|$ magnitude in comparison with the regime "cos + cos".

Though the obtained results concerning the higher harmonics are interesting, the higher harmonics excited in the four-phonon processes are usually small (Figs. 8, 10, 13 and 15). For example even in the propagation of a pure sinusoidal wave the third harmonic amplitude is less than 10% of the fundamental (Fig. 6). These are the ω-wave and the 2ω-wave that commonly dominate in the total acoustic signal (see the insets in Figs. 8, 10, 13 and 15). Consequently, the most important is to analyze the mutual influence of these waves in the process of frequency mixing. In Fig. 16 we present the results of this analysis in the case $\Delta\varphi = 0$ ("sin + sin"). The dependence of the amplitude of one wave on the amplitude of another one is evaluated at different distances from the boundary.

The examination of the results in Fig. 16 leads to the conclusion that at short propagation distances the increase in the amplitude of either ω-wave (A_1) or the 2ω-wave

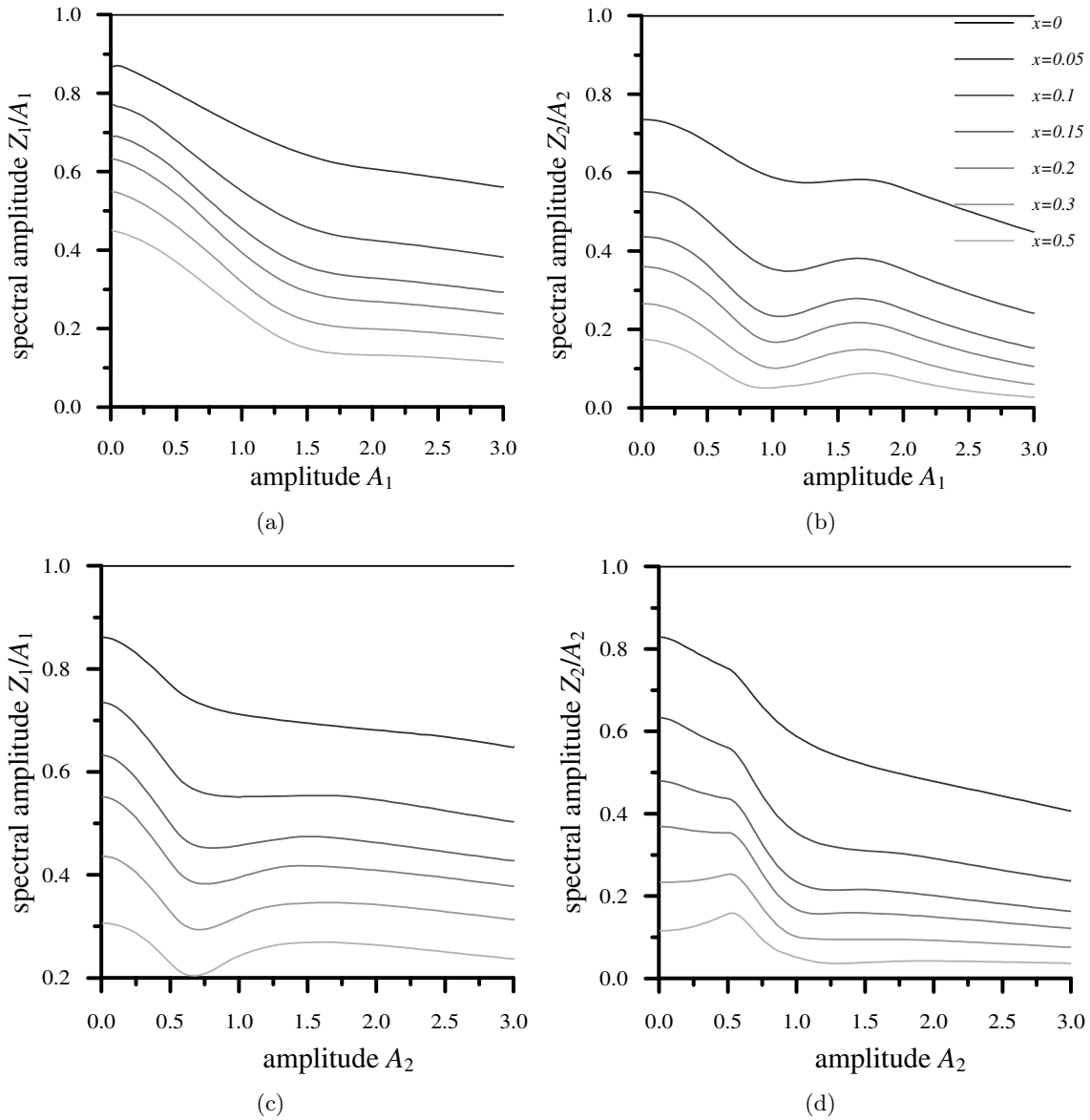

Fig. 16. The normalized spectral amplitudes Z_1/A_1 (a), (c) and Z_2/A_2 (b), (d) for different depths x as functions of the amplitude A_1 ($A_2 = 1 = \text{const.}$) (a), (b) and as functions of A_2 ($A_1 = 1 = \text{const.}$) (c), (d), calculated for the initial signal $s(x = 0, \tau) = A_1 \sin 2\pi f_1 \tau + A_2 \sin 2\pi f_2 \tau$, $f_1 = 1, f_2 = 2$.

(A_2) usually induces additional absorption ($\partial(Z_1/A_1)/\partial A_1 < 0$, $\partial(Z_1/A_1)/\partial A_2 < 0$, $\partial(Z_2/A_2)/\partial A_2 < 0$). Only the dependence of the 2ω-wave amplitude on the amplitude of the ω-wave exhibits the regime of the induced transparency ($\partial(Z_2/A_2)/\partial A_1 > 0$) in the neighborhood of $A_1 \approx 1.5$ (Fig. 16(b)). At larger propagation distances this induced transparency regime becomes even more pronounced, and the intervals of the induced transparency are also predicted for the influence of 2ω-wave on the ω-wave as well (Fig. 16(c),

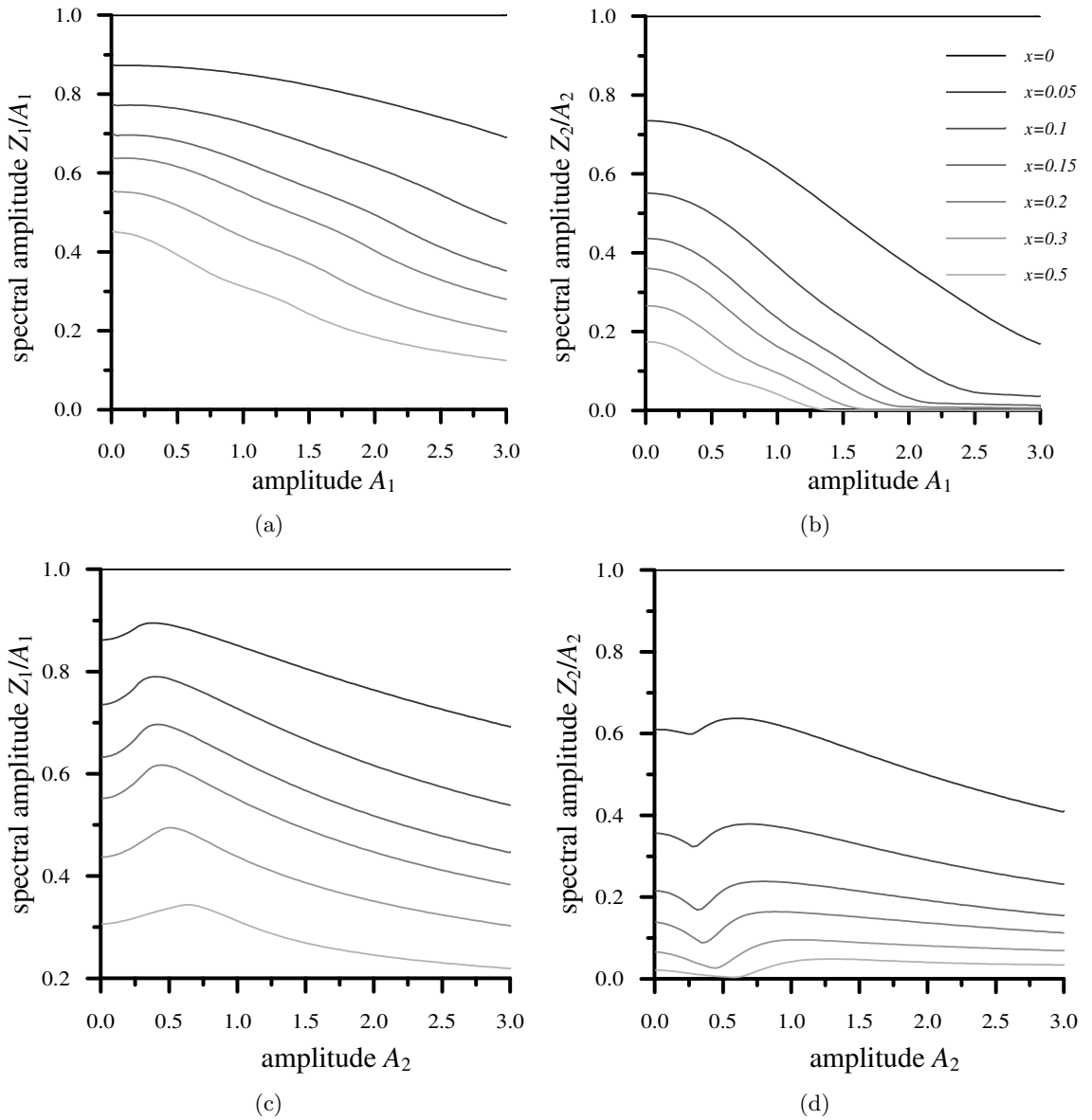

Fig. 17. The normalized spectral amplitudes Z_1/A_1 (a), (c) and Z_2/A_2 (b), (d) for different depths x as functions of the amplitude A_1 ($A_2 = 1 = \text{const.}$) (a), (b) and as functions of A_2 ($A_1 = 1 = \text{const.}$) (c), (d), calculated for the initial signal $s(x = 0, \tau) = A_1 \cos 2\pi f_1 \tau + A_2 \cos 2\pi f_2 \tau, f_1 = 1, f_2 = 2$.

$x \geq 0.2$, $A_2 \approx 1$). Moreover, the self-induced transparency is found for the 2ω-wave in the field of the ω-wave at sufficiently large distances (Fig. 16(d), $\partial(Z_2/A_2)/\partial A_2 > 0$ for $x \geq 0.3$ and $A_2 \leq 0.5$).

In Fig. 17 we illustrate the mutual influence of the ω- and 2ω-waves in the case $\Delta\varphi = \pi/4$ ("cos + cos"). Comparison of Figs. 16 and 17 clearly indicates the dependence of the analyzed processes on the phase between the input waves. In the regime $\Delta\varphi = \pi/4$ the increase

of the ω-wave amplitude induces additional absorption of both ω- and 2ω-waves at all tracked distances (Fig. 17(a,b)). At the same time the increase of the 2ω-wave amplitude can diminish absorption of both ω- and 2ω-waves even at shortest propagation distances. Induced transparency ($\partial(Z_1/A_1)/\partial A_2 > 0$) is predicted numerically for $A_2 \leq 0.5$ (Fig. 17(c)). Self-induced transparency for the 2ω-wave ($\partial(Z_2/A_2)/\partial A_2 > 0$) in the presence of the ω-wave is expected in the interval of A_2 values that depends on the propagation distance (Fig. 17(d)).

The numerically obtained predictions concerning the existence of the induced transparency effects even at the shortest propagation distances indicate that these effects (at least near the boundary) are not due to the wave spectrum transformation but rather due to the peculiar features of local nonlinear hysteretic absorption in the process of two frequency mixing. This gave us an idea to analyze the local hysteretic absorption of both ω- and 2ω-oscillations at the boundary $x = 0$. Fortunately in the case $\Delta\varphi = \pi/4$ the analytical description of the local hysteretic absorption is possible in addition to numerical (providing additional insight in the physics of the phenomena and an additional opportunity to test our numerical algorithm).

5. Analytical and Numerical Analysis of Local Nonlinear Hysteretic Absorption

In order to get better physical insight in the obtained results of numerical simulations of the nonlinear wave propagation (discussed in Sec. 4) we present below some analytical results related to local hysteretic absorption in the considered process of ω and 2ω interaction. Surely the harmonics that are generated in the nonlinear wave propagation of the primary waves at ω and 2ω do also contribute to the process of nonlinear hysteretic absorption, so that the applicability of the below presented analytical results is limited to the vicinity of the boundary $x = 0$ (where the higher harmonics and their inverse influence on ω and 2ω are negligible). However, comparison with the analytical results definitely indicates that the numerically predicted effects of the induced transparency and induced absorption near the boundary are peculiar features of the hysteretic absorption (and not those of frequency mixing and energy redistribution among ω, 2ω and higher harmonics).

Compact analytical solutions can be obtained for the boundary signal in Eq. (4.2) ($\Delta\phi = \pi/4$). In the following we use the notation $\theta = 2\pi\tau$ in the arguments of the signals in Eqs. (4.1) and (4.2). A simple analysis of Eq. (4.2) indicates that the strain is "simplex" if the nondimensional parameter $p = A_1/4A_2$ satisfies the inequality $p > 1$. In other words, the amplitude A_2 of the "high-frequency" component at 2ω should be sufficiently small in comparison with the amplitude of the "low-frequency" component at ω ($A_2 < A_1/4$). In the simplex regime the process in Eq. (4.2) has the single maximum ($s_{\min}^{abs} = A_1 + A_2$ at $\theta = 2\pi n$, $n = 0, \pm1, \pm2, \ldots$) and the single minimum ($s_{\min}^{abs} = -A_1 + A_2$ at $\theta = (2n+1)\pi$, $n = 0, \pm1, \pm2, \ldots$) over a wave period ($(2n-1)\pi \leq \theta < (2n+1)\pi$, $n = 0, \pm1, \pm2, \ldots$). In the following we consider for definiteness the period $-\pi \leq \theta < \pi$.

The process in Eq. (4.2) is "complex" in the parameter region $p < 1$. In the complex

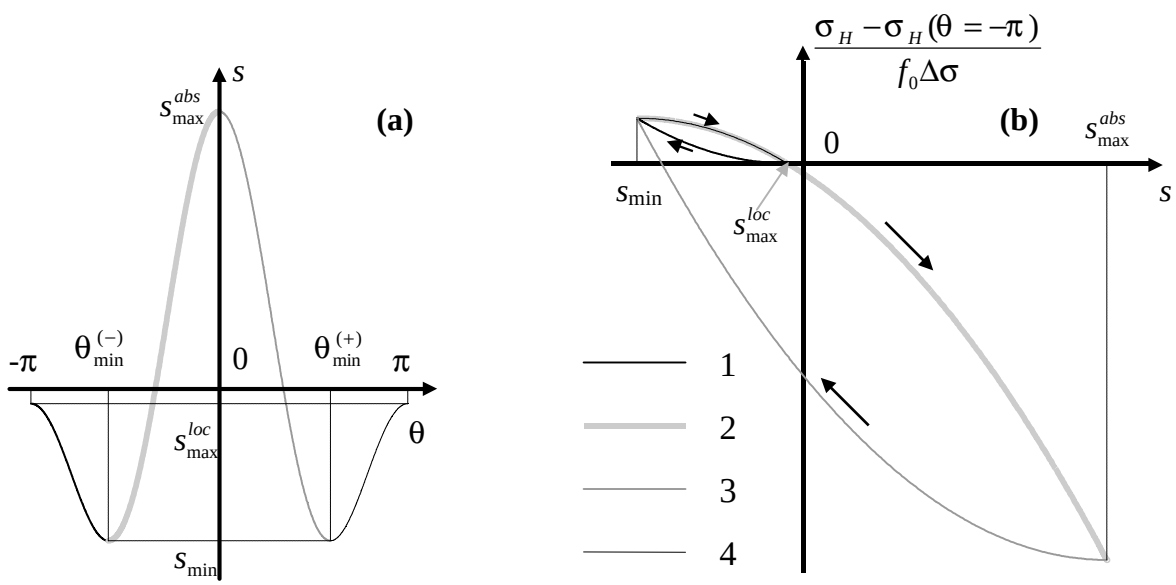

Fig. 18. The normalized hysteretic stress (b) as a function of strain (a) for the process $s = A_1\cos\theta + A_2\cos 2\theta$. The intervals $-\pi \le \theta \le \theta^{(-)}_{\min}, \theta^{(-)}_{\min} \le \theta \le 0$, $0 \le \theta \le \theta^{(+)}_{\min}$, $\theta^{(+)}_{\min} \le \theta \le \pi$ are marked by different line styles (1, 2, 3, 4, respectively).

process the amplitude and the position of the absolute maximum coincide with those in the simplex process (see Fig. 18(a)), i.e. $s^{abs}_{\max} = s(\theta = 0) = A_1 + A_2 = A_2(1 + 4p)$. In contrast, the absolute minimum of the simplex process transforms into the local maximum of the complex process $s^{\mathrm{loc}}_{\max} = s(\theta = \pi) = -A_1 + A_2 = A_2(1 - 4p)$. Additionally two equal minima appear over a period $s_{\min} = s(\theta = \theta^{(\pm)}_{\min} = \pm\arccos(-p)) = -A_2(1 + 2p^2) < s^{\mathrm{loc}}_{\max}$. As a result in the considered complex process we have two maximas and two minimas over a period (Fig. 18(a)).

Applying the rules formulated in Sec. 2 it is straightforward to find the form of the nonlinear contribution to elastic modulus $\partial\sigma/\partial s$ for the considered process in Eq. (4.2). Applying Eqs. (2.9) and (2.10) in the simplex regime ($p > 1$) we get:

$$\frac{\partial\sigma_H}{\partial s} = -f_0\Delta\sigma \times \begin{cases} s - s^{abs}_{\min}, & -\pi < \theta < 0\,, \\ s^{abs}_{\max} - s, & 0 < \theta < \pi\,. \end{cases} \tag{5.1}$$

Integration of Eq. (5.1) provides the description of the nonlinear hysteretic contribution to stress:

$$\sigma_H = \begin{cases} \sigma(\theta = -\pi) - f_0\Delta\sigma(s - s^{abs}_{\min})^2/2, & -\pi \le \theta \le 0\,, \\ \sigma(\theta = 0) + f_0\Delta\sigma(s^{abs}_{\max} - s)^2/2, & 0 \le \theta \le \pi\,. \end{cases} \tag{5.2}$$

The relation between the integration constants $\sigma_H(\theta = -\pi)$ and $\sigma_H(\theta = 0)$ is provided either by the continuity of the stress at $\theta = 0$ (where $s = s^{abs}_{\max}$) or by the periodicity of the

stress $\sigma_H(\theta=-\pi)=\sigma_H(\theta=\pi)$ (note that $s(\theta=-\pi)=s(\theta=\pi)=s_{\min}^{abs}$):

$$\sigma_H(\theta=0)=\sigma_H(\theta=-\pi)-f_0\Delta\sigma(s_{\max}^{abs}-s_{\min}^{abs})^2/2\,. \tag{5.3}$$

The solution for the hysteretic nonlinear stress in (5.2)–(5.3) is sufficient for the evaluation of the hysteretic absorption because the undetermined component $\sigma_H(\theta=-\pi)$ of the stress is constant over a period and, therefore, does not contribute to losses.

The generalization of the results in (5.1)–(5.3) for the complex regime ($p<1$) is also straightforward

$$\frac{\partial\sigma_H}{\partial s}=-f_0\Delta\sigma\times\begin{cases} s_{\max}^{\rm loc}-s, & -\pi<\theta<\theta_{\min}^{(-)}\,,\\ s-s_{\min}, & \theta_{\min}^{(-)}<\theta<0\,,\\ s_{\max}^{abs}-s, & 0<\theta<\theta_{\min}^{(+)}\,,\\ s-s_{\min}, & \theta_{\min}^{(+)}<\theta<\pi\,. \end{cases}$$

$$\sigma_H=\sigma_H\big|_{\theta=-\pi}-\frac{f_0\Delta\sigma}{2}\times\begin{cases} -(s_{\max}^{\rm loc}-s)^2, & -\pi\le\theta\le\theta_{\min}^{(-)}\,,\\ -(s_{\max}^{\rm loc}-s_{\min})^2+(s-s_{\min})^2, & \theta_{\min}^{(-)}\le\theta\le 0\,,\\ -(s_{\max}^{\rm loc}-s_{\min})^2+(s_{\max}^{abs}-s_{\min})^2-(s_{\max}^{abs}-s)^2, & 0\le\theta\le\theta_{\min}^{(+)}\,,\\ -(s_{\max}^{\rm loc}-s_{\min})^2+(s-s_{\min})^2, & \theta_{\min}^{(+)}\le\theta\le\pi\,. \end{cases} \tag{5.4}$$

In Fig. 18(b) we present the stress/strain hysteretic curve with a minor loop predicted in Eq. (5.4) for the complex process ($p<1$) of ω and 2ω mixing. Using the obtained form of the nonlinear stress relationship we evaluate directly the energy density loss (E) over a period. Furthermore, the overall hysteretic absorption is readily separated into the losses over a period at frequency ω (E_1) and at 2ω (E_2):

$$E=\oint\sigma_H(s)ds=\int_{-\pi}^{+\pi}\sigma_H[s(\theta)]\cdot(-A_1\sin\theta-2A_2\sin 2\theta)d\theta\equiv E_1+2E_2\,. \tag{5.5}$$

Here $\oint$ denotes the integration over a period of strain variation,

$$E_1=-A_1\int_{-\pi}^{+\pi}\sigma_H[A_1\cos\theta+A_2\cos 2\theta]\cdot\sin\theta d\theta\,,$$

$$E_2=-A_2\int_{-\pi}^{+\pi}\sigma_H[A_1\cos\theta+A_2\cos 2\theta]\cdot\sin 2\theta d\theta\,.$$

The factor "2" on the right-hand-side of Eq. (5.5) takes into account that two periods of the 2ω wave contribute to the hysteretic loss in a single period of total strain variation. We

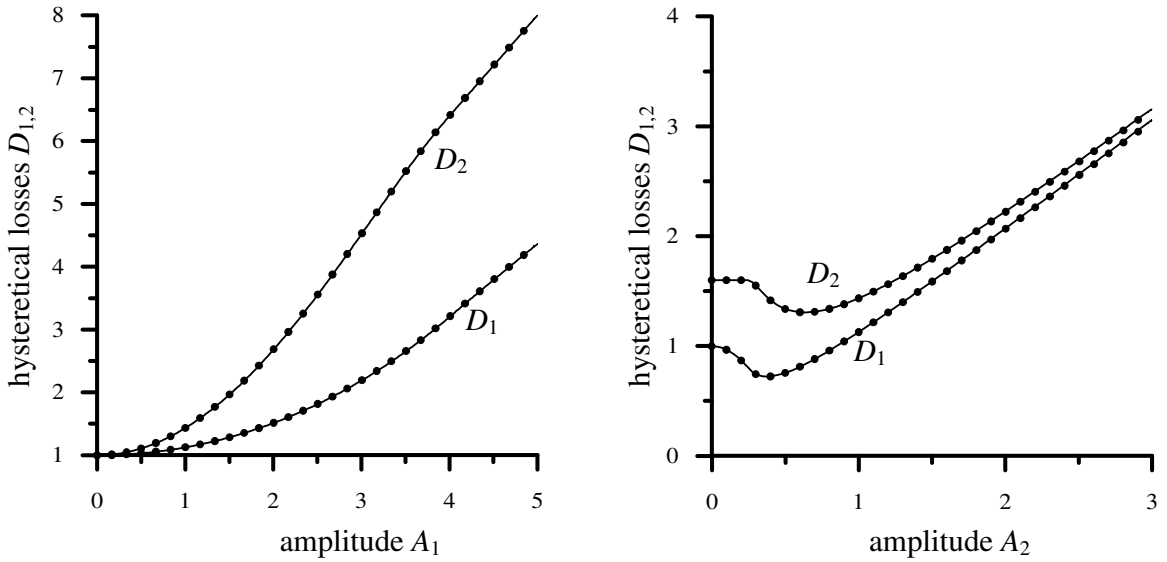

Fig. 19. Hysteretical losses D_1 and D_2 for different depths x as functions of the amplitude A_1 ($A_2 = 1 =$ const.) (a) and as functions of $A_2(A_1 = 1 = \text{const.})$, (b) calculated for the initial signal $s(x = 0, \tau) = A_1 \cos 2\pi f_1 \tau + A_2 \cos 2\pi f_2 \tau, f_1 = 1, f_2 = 2$. The points represent analytical results.

also introduce the notations W_1 and W_2 for the energy densities at ω and 2ω averaged over a wave period

$$W_1 = \frac{1}{2\pi}\rho_0 c_0^2 \int_{-\pi}^{\pi} (A_1 \cos\theta)^2 d\theta = \frac{1}{2}\rho_0 c_0^2 A_1^2 \,,$$

$$W_1 = \frac{1}{2\pi}\rho_0 c_0^2 \int_{-\pi}^{\pi} (A_2 \cos 2\theta)^2 d\theta = \frac{1}{2}\rho_0 c_0^2 A_2^2 \,,$$

and define the acoustic decrements (i.e. the inverse quality factors) characterizing the nonlinear hysteretic absorption at frequencies ω and 2ω by $D_{1,2} = E_{1,2}/2W_{1,2}$.

The evaluation of the decrements is carried out analytically. The final result is convenient to be presented in normalized variables $D_{1,2} = D_{1,2}/D^0$, $A_{1,2} = A_{1,2}/s^0$, where s^0 is the characteristic strain amplitude and $D^0 = 4f_0 \Delta\sigma s^0/(3\rho_0 c_0^2)$ is the characteristic decrement, which corresponds to hysteretic losses in a simplex sinusoidal process with strain amplitude s^0. For the description of the nonlinear hysteretic losses at frequency ω we derived

$$D_1 = \begin{cases} A_1 \left(1 - \dfrac{1}{5p^2}\right), \quad p > 1 \quad \text{(simplex)}\,, \\ A_2 \left(1 + 2p^2 + \dfrac{1}{5}p^4\right), \quad p < 1 \quad \text{(complex)}\,. \end{cases} \tag{5.6}$$

The dependencies of the decrement D_1 on the amplitudes A_1 and A_2 of the input waves are illustrated in Figs. 19(a) and (b). The transition from the simplex to the complex regime (or

vice versa) clearly influences the decrement of the 2ω wave. It manifests itself in the kinks in the dependence $D_2 = D_2(A_1)$ at $A_1 = 4$ (Fig. 19(a)) and in the dependence $D_2 = D_2(A_2)$ at $A_2 = 0.25$ (Fig. 19(b)). However, the influence of the simplex-complex transition on the decrement of the ω wave looks much less pronounced.

In accordance with Eq. (5.6) when the component at 2ω is negligibly small ($p \to \infty$) the decrement at ω is proportional to its amplitude A_1. We recover a classical feature ($D_1 \propto A_1$) of the hysteretic amplitude-dependent absorption of monochromatic wave.[1–4,20] When the amplitude A_2 increases then Eq. (5.6) predicts that in the simplex regime ($p > 1$) the injection of 2ω causes the decrease of the decrement at ω. Qualitatively, for the "low-frequency" signal at ω, the signal at 2ω can be treated as a "high-frequency" signal and called the dither.[32–34] Thus we can say that in the simplex regime the injection of a dither induces the transparency for the wave at frequency ω. This effect is predicted here for the first time. In Ref. 35 it has been demonstrated that in the medium with the hysteretic quadratic nonlinearity a weak counter-propagating wave induces transparency for a strong wave of the same frequency. The predicted effect of the absorption decrease was proportional to the square of the weak wave amplitude (Eq. (29) in Ref. 35) similar to the result in Eq. (5.6) where $D_1(\text{simplex}) = A_1 - (16/5)(A_2^2/A_1)$. However, the results of Ref. 35 cannot be directly applied for the waves propagating in the same direction and of different frequencies. The theory of the dithers in the materials with hysteretic quadratic nonlinearity in the case of simplex processes might be developed by extending the formalism of the successive approximations[31] proposed earlier for the analysis of the absorption induced by a strong pump wave for the weak probe wave propagating in the same direction. It could be an interesting perspective for the future research in particular due the expected from Ref. 31 the possible dependence of the phenomenon on the relative phase of the low-frequency and the high-frequency signals.

In line with Eq. (5.6) the transition to complex regime with decreasing parameter p (increasing A_2 for a fixed A_1) introduces additional losses at frequency ω. These losses with increasing A_2 first compensate the transparency induced by the dither properties of the 2ω-wave and finally lead to induced hysteretic absorption proportional to A_2. The latter regime in the limit $A_2 \gg A_1$ was predicted earlier in Ref. 31. Importantly the analytical result in (5.6) describes a peculiar transition between the limiting cases ($A_2 \ll A_1$ and $A_2 \gg A_1$) both evaluated earlier. In this transition the competition of the properties of 2ω-wave as a dither and its ability to create internal loop in the hysteretic stress/strain relationship leads to the existence of the critical amplitude A_2^{cr1}, which provides minimum of losses at frequency ω ($A_2^{\text{cr1}} = A_1/(4\sqrt{5/3}\sqrt{\sqrt{1+3/5}-1}) \approx A_1/2.7$. The dependence of D_1 on A_2 for a fixed A_1 is presented in Fig. 19(b).

In contrast to the nonmonotonous behavior of $D_1(A_2)$, decrement D_1 as a function of A_1 continuously rises with increasing A_1 ($\partial D_1/\partial A_1 \geq 0$, see Fig. 19(a)). The transition between the regime $A_1 \ll A_2$ (where the absorption of ω induced by 2ω dominates, $D_1 \propto A_2$ [31]) and the regime $A_1 \gg A_2$ (dominated by self-absorption of ω, $D_1 \propto A_1$ [1,20]) is monotonous. The transition from complex to simplex regime (disappearance of the internal loop when $A_1 = 4A_2$) has just a minor influence on this monotonic behavior.

In a similar way for the nonlinear hysteretic losses at frequency 2ω we derived

$$D_2 = \begin{cases} \dfrac{8}{5}A_1, & p > 1 \quad \text{(simplex)}\,, \\ A_2\left(1 + 7p^2 - p^4 - \dfrac{3}{5}p^6\right), & p < 1 \quad \text{(complex)}\,. \end{cases} \tag{5.7}$$

In accordance with (5.7) the absorption of 2ω in the simplex regime ($p > 1$, $A_2 < A_1/4$) is induced by the higher amplitude wave at frequency ω (induced absorption of a weak signal wave is proportional to the amplitude of a pump wave $D_2 \propto A_1$ as discussed in Ref. 31). Importantly Eq. (5.7) predicts the complete absence of the hysteretic self-absorption of the 2ω wave in the absence of the internal (minor) loop (i.e. $\partial D_2/\partial A_2 = 0$ in the simplex process). Amazing prediction contained in Eq. (5.7) is that the transition to complex regime with increasing A_2 (for a fixed A_1) leads to the diminishing of losses at frequency 2ω. It means that the appearance of self-absorption (which leads to increase of D_2) is initially overcompensated by the fall in the absorption of 2ω induced by the presence of the pump wave at frequency ω. Thus the formation of the internal loop with increasing A_2 is accompanied by the effect of self-induced transparency ($\partial D_2/\partial A_2 \leq 0$ for $A_2 \geq A_1/4$, see Fig. 19(b)). Surely with further increase of A_2 the self-absorption of the 2ω wave becomes more and more important, and in the limiting regime $p \ll 1$, $A_2 \gg A_1$ Eq. (5.7) predicts the dominance of the hysteretic self-absorption ($D_2 \propto A_2$ in accordance with the well-established results[1,20]). This peculiar dependence of D_2 on A_2 is illustrated in Fig. 19(b). The minimum of the losses at 2ω takes place at critical amplitude $A_2^{\mathrm{cr}2} = A_1/(4\sqrt{2/\sqrt{3}-1}) \approx A_1/1.6$, which is different from $A_1^{\mathrm{cr}1}$. The transition between the regime of self-absorption ($D_2 \propto A_2$ when $A_1 \ll A_2$) to the regime of the pump-induced absorption ($D_2 \propto A_1$ when $A_1 \gg A_2$) with increasing amplitude of the wave at frequency ω is monotonous $\partial D_2/\partial A_1 \geq 0$ (see Fig. 19(a)).

From the analysis presented above we conclude that (for the input signal in Eq. (4.2)) the decrements $D_{1,2}$ depend monotonously on the amplitude of the low-frequency (ω) wave and nonmonotonously on the amplitude of the high-frequency (2ω, dither) wave. The peculiar effects of the induced transparency and absorption are related to the properties of the 2ω-wave as a dither and the influence of the transition from simplex to complex regime on the induced absorption. All the effects predicted above for the local hysteretic absorption at the boundary $x = 0$ are reflected in the evaluated numerically transformations accompanying nonlinear wave propagation (see Fig. 17). In particular the transparency induced by a small-amplitude 2ω-wave for the propagation of the ω-wave (Fig. 17(c)) is due to the dither properties of the higher frequency wave for this particular phasing ($\Delta\phi = \pi/4$) (Fig. 19(b)). The self-induced transparency of the 2ω-wave (Fig. 17 (d)) is initiated by the formation of the minor loop and the transition from the simplex to complex process with increasing A_2 (Fig. 19(b)).

In Fig. 20 the results of the numerical calculation of the local hysteretic losses in the case $\Delta\phi = 0$ (Eq. (4.1), "sin + sin") are presented. The most of the kinks in the dependences of

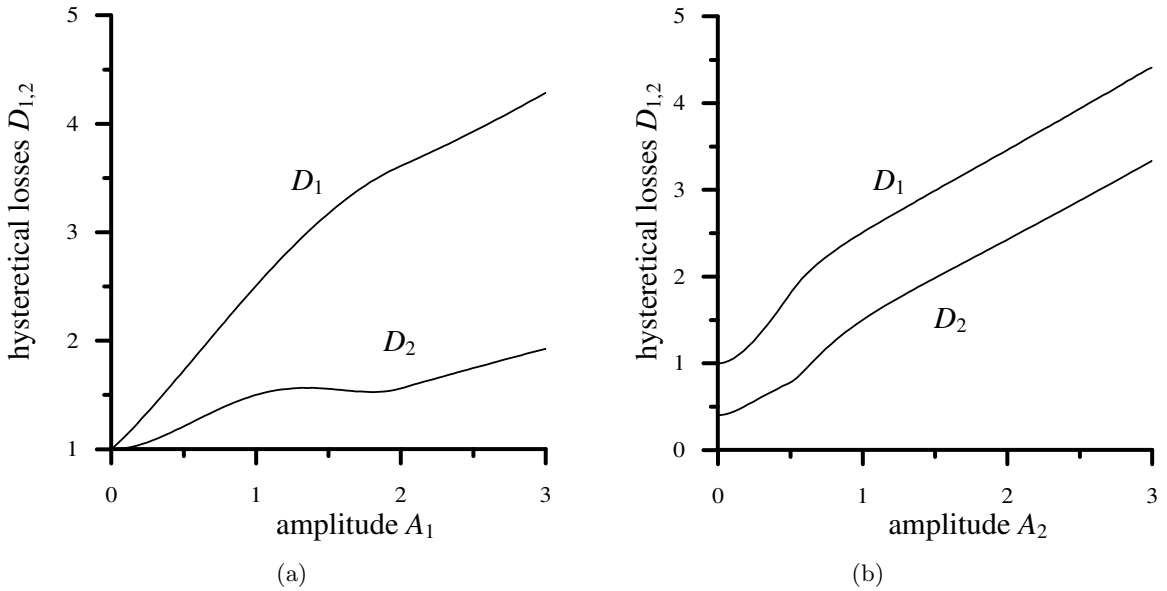

Fig. 20. Hysteretical losses D_1 and D_2 for different depths x as functions of the amplitude A_1 ($A_2 = 1 =$ const.) (a) and as functions of A_2 ($A_1 = 1 =$ const), (b) calculated for the initial signal $s(x = 0, \tau) = A_1 \sin 2\pi f_1 \tau + A_2 \sin 2\pi f_2 \tau$, $f_1 = 1, f_2 = 2$.

the decrements D_1 and D_2 on the amplitudes of the input waves in Fig. 20 can be related to the transition between the simplex and the complex regimes of the boundary oscillations. There is a clear correspondence between these predictions and the phenomena of the induced absorption and transparency at short propagation distances shown in Fig. 16. In particular, the regime of the diminishing absorption of the 2ω-wave with the increasing amplitude of the ω-wave can be clearly identified for the same interval $1.5A_2 \leq A_1 \leq 2A_2$ both in Fig. 16(b) and in Fig. 20(a). The maximum amplitude A_1 (the upper boundary $A_1 \approx 2A_2$) for this regime of the induced transparency is related to the transition from the complex to the simplex regime in the acoustic emission from the boundary with the increasing amplitude of the ω-wave. Interestingly the character of the dither effect (describing the influence of the lower in amplitude higher frequency wave on the higher in amplitude lower frequency wave) has changed the sign in the case $\Delta\phi = 0$ in comparison with the previous limiting case $\Delta\phi = \pi/4$. Injection of a weak 2ω-wave causes additional absorption (induced absorption) of the ω-wave ($\partial D_1/\partial A_2 > 0$ for $A_2 \ll A_1$). The role of the two signals phasing on the process of the nonlinear hysteretic absorption requires additional more detailed investigation in the future.

6. Qualitative Discussion of the Effects Related to Nonlinear Hysteretic Absorption

In the previous section it was demonstrated that the major contribution to the mutual influence of the ω- and 2ω-waves at short propagation distances is provided by the process

of the nonlinear hysteretic absorption. Unfortunately, deeper interpretation of the obtained results is very difficult at least at the current level of our knowledge. Even the results for the local hysteretic absorption presented in Figs. 19 and 20 look at first glance counterintuitive. For example, with the analytical description of the stress/strain relationship Eqs. (5.2)–(5.4) (simply by examining the contributions to the integral in Eq. (5.5)) the following can be easily understood. Due to the formation of the internal loop the amplification of the 2ω-wave in the simplex wave (that takes place near the absolute minima in $\theta = (2n+1)\pi$ in the case $\Delta\phi = \pi/4$) changes in the complex regime for its absorption in the same neighborhood of $\theta = (2n+1)\pi$. This is related to the change in the character of the extremum in $\theta = (2n+1)\pi$ from the minimum in the simplex regime to the local maximum in the complex regime. So the formation of the internal loop leads to the absorption increase for the 2ω-wave in the time intervals where the system moves along the internal loop. This conclusion is also in accordance with the expectation that in the asymptotic case $A_2 \gg A_1$ this internal loop should provide half of the self-absorption of the 2ω-wave. However, this prediction makes the result in Fig. 19(b), where the formation of the internal loop for $A_2 \geq 0.25A_1$ leads to the decrease of the decrement D_2, at first glance counterintuitive. To explain the dependence $D_2 = D_2(A_2)$ in Fig. 19(b) (obtained both numerically and analytically) we have to admit that in reality the formation of the internal loop has a pronounced influence on the processes taking place along the major loop. And, in fact, the transparency induced for the 2ω-wave along the major loop overcompensates the absorption induced along the minor loop. Finally this conclusion will stop looking counterintuitive if we remind that there is a memory in the considered system in particular of the latest extremum. Consequently, the formation of the minor loop by modifying the amplitudes of the extrema should have influence not only on the local processes (along the internal loop), but on the processes along the major loop as well. This influence results in the modification of the hysteretic absorption process over the complete wave period.

There is an additional argument providing indication that in the neighborhood of the transition from the simplex to the complex regime these are the processes along the main hysteresis loop that play the major role in the case $\Delta\phi = \pi/4$ ("$\cos + \cos$"). The magnitude of the contribution to the absorption (amplification) coming from the internal loop is small due to the fact that the minor loop in this regime is located near the extrema of both ω and 2ω strain waves. Because of this the differential (ds) is small in Eq. (5.5) along the internal loop. So the dominant role of the major loop is expected.

Let us apply the qualitative arguments listed above to the analysis of the regime $\Delta\phi = 0$ ("$\sin + \sin$", Eq. (4.1)). By the examination of Fig. 20(b) we conclude that the variation in the absorption of the waves caused by the formation of the internal loop are again in anti-phase. Indeed near the transition ($A_2 = 0.5A_1$) with the increasing 2ω-wave amplitude the rate of the D_1 variation decreases while the rate of the D_2 variation rises. However, the sign of the absorption variation does not change (the regime of the induced transparency is not predicted in Fig. 20(b)). We may conclude that in this regime the leading role in the sound absorption even after the formation of the minor loop plays the interval of the in-phase variation of the strain in ω- and 2ω-waves ($(2n - 1/2)\pi < \theta < (2n + 1/2)\pi$). This causes

in-phase variation in the absorption of ω- and 2ω-waves even after the transition from simplex to complex regime (with increasing A_2). This conforms to our intuition because for the "sin + sin" regime near the transition we have in the interval $(2n - 1/2)\pi < \theta < (2n + 1/2)\pi$ both the absolute maximum and the absolute minimum of the total strain that are influenced but do not change their character when the minor loop is formed. We remind that these are the extrema of the wave profile where (in accordance with the time-domain analysis of the wave profile evolution) the hysteretic absorption is concentrated. So we arrive to the conclusion that the temporal separation of the internal loop from the absolute extrema (compare the regimes $\Delta\phi = 0$ and $\Delta\phi = \pi/4$) reduces the qualitative influence of its formation on the losses both at ω and 2ω frequencies (compare Figs. 20(b) and 19(b)).

The kinks in the variation of the losses in the regime $\Delta\phi = 0$ due to the transition between the complex and the simplex regimes are also observed when the amplitude of the ω-wave is varied near $A_1 = 2A_2$ (Fig. 20(a)). The changes in the rate of D_1 and D_2 variation are again in anti-phase. We underline here that the anti-phase variation in the rate of the absorption at ω and 2ω frequencies due to the transition between the simplex and complex regimes is the general feature of the investigated phenomenon related to the fact that the minor loop appears always in the time-interval of the anti-phase variation of strain in ω- and 2ω-waves (that is where in one wave it diminishes while in the other wave it increases, or vice versa). It can be seen (Fig. 20(a)) that the regime of the induced transparency for the 2ω-wave can be induced by the increasing amplitude of the ω-wave just below the transition from the complex to the simplex regime ($1.5A_2 \leq A_1 \leq 2A_2$). Clearly in this interval of the ω-wave amplitudes the diminishing of the 2ω-wave absorption due to the shrinkage of the minor loop with increasing A_1 overcomes increasing absorption induced by the increase of the major loop. The regime of the induced transparency terminates at $A_1 = 2A_2$ when with increasing A_1 the internal loop disappears. Consequently, the conclusions drawn just in the previous paragraph are not completely general. Even in the limiting case $\Delta\phi = 0$ the rate of the absorption variation can change the sign due the transition between the simplex and the complex regimes, although the influence of the transition on the absorption in the system is less pronounced in the comparison with the regime $\Delta\phi = \pi/4$.

7. Conclusions

The numerical code is developed for the analysis of plane acoustic wave propagation in the nonlinear mesoscopic materials. The results of both numerical and analytical investigation of the wave frequency mixing process in materials with hysteretic quadratic nonlinearity revealed multiple complex phenomena due to hysteresis and memory in the considered materials. Most of the results were obtained for the case of the ω-wave the 2ω-wave mixing.

The transformation of the wave profile and the wave spectrum in nonlinear wave propagation are investigated numerically and interpreted. It is demonstrated that for some phase shifts between the ω- and 2ω-input waves the efficiency of the forth harmonic excitation can exceed the efficiency of the third harmonic excitation. The transformation of a complex

wave into a simplex wave in nonlinear propagation is demonstrated and the dependence of the process on the relative phase of the ω- and 2ω-waves is explained by the influence of the relative phase on the efficiency of the nonlinear hysteretic absorption at local extrema.

It is established that at short propagation distances the interaction of the ω- and 2ω-waves is mainly through the mechanism of the nonlinear hysteretic absorption and is not strongly influenced by the process of new spectral components generation and their inverse influence on the input waves. Peculiar regimes of the induced transparency (where the increasing amplitude of the $\omega(2\omega)$-wave leads to fall in the absorption of $2\omega(\omega)$-wave) are predicted both numerically and analytically, and qualitatively interpreted. The regime of the self-induced transparency (where in the presence of the ω-wave the increasing amplitude of the 2ω-wave induces fall in the absorption of the 2ω-wave) is also demonstrated and explained qualitatively. The role of the transition from the emission of the simplex wave to the emission of the complex wave (or vice versa) in the process of the induced absorption and transparency is identified.

The obtained results are expected to find applications in the nondestructive evaluation of the mesoscopic materials and in seismology.

Acknowledgments

One of us (V. A.) gratefully acknowledges the Fellowship from the University of Maine (France, 2001–2002) and the Grant from the Foundation for Scientific Research (Belgium, 2002–2003). We also thank Prof. Koen Van Den Abeele for numerous friendly discussions.

References

1. V. E. Nazarov, L. A. Ostrovsky, I. A. Soustova and A. M. Sutin, *Sov. Phys. Acoust.* **34** (1988) 284.
2. V. E. Nazarov, L. A. Ostrovsky, I. A. Soustova and A. M. Sutin, *Phys. Earth Planet. Inter.* **50** (1988) 65.
3. V. E. Nazarov, *Sov. Phys. Acoust.* **37** (1991) 75.
4. V. E. Nazarov, *J. Acoust. Soc. Am.* **107** (2000) 1915.
5. V. E. Nazarov and S. V. Zimenkov, *Acoust. Lett.* **16** (1993) 218.
6. P. A. Johnson, B. Zinszner and P. N. J. Rasolofosaon, *J. Geophys. Res.* **101** (1996) 11553.
7. B. Zinszner, P. A. Johnson and P. N. J. Rasolofosaon, *J. Geophys. Res.* **102** (1997) 8105.
8. V. E. Nazarov, A. V. Radostin and I. A. Soustova, *Sov. Phys. Acoust.* **48** (2002) 85.
9. J. K. Na and M. A. Breazeale, *J. Acoust. Soc. Am.* **95** (1994) 3213.
10. R. A. Guyer and P. A. Johnson, *Phys. Today* **52** (1999) 30.
11. V. Yu. Zaitsev and P. Sas, *Acustica-Acta Acustica* **86** (2000) 429.
12. V. Yu. Zaitsev, V. E. Nazarov and I. Yu. Belyaeva, *Acoust. Phys.* **47** (2001) 178.
13. V. Zaitsev, V. Gusev and B. Castagnede, *Phys. Rev. Lett.* **89** (2002) 105502.
14. D. J. Holcomb, *J. Geophys. Res.* **86** (1981) 6235.
15. R. A. Guyer, K. R. McCall and G. N. Boitnott, *Phys. Rev. Lett.* **74** (1995) 3491.
16. F. Preisach, *Z. Phys.* **94** (1935) 277.
17. I. D. Mayergoyz, *J. Appl. Phys.* **57** (1985) 3803.
18. I. D. Mayergoyz, *Phys. Rev. Lett.* **56** (1986) 1518.

19. M. A. Krasnosel'skii and A. V. Pokrovskii, *Systems with Hysteresis* (Nauka, Moscow, 1983; Springer, Berlin, 1989).
20. V. Gusev, C. Glorieux, W. Lauriks and J. Thoen, *Phys. Lett.* **A32** (1997) 77.
21. V. Gusev, W. Lauriks and J. Thoen, *J. Acoust. Soc. Am.* **103** (1998) 3216.
22. V. Gusev, *J. Acoust. Soc. Am.* **107** (2000) 3047.
23. K. Van Den Abeele, P. A. Johnson, R. A. Guyer and K. R. McCall, *J. Acoust. Soc. Am.* **101** (1997) 1885.
24. O. V. Rudenko and S. I. Soluyan, *Theoretical Foundations of Nonlinear Acoustics* (Consultants Bureau, New York, 1976).
25. R. Kurant and K. Friedrichs, *Supersonic Flow and Shock Waves* (Interscience, New York, 1948).
26. V. E. Gusev and A. A. Karabutov, *Laser Optoacoustics*, Chap. 6 (AIP, New York, 1993).
27. M. Scalerandi, V. Agostini, P. P. Delsanto, K. Van Den Abeele and P. A. Johnson, *J. Acoust. Soc. Am.* **113** (2003) 3049–3059.
28. M. Scalerandi, P. P. Delsanto and P. A. Johnson, *J. Phys.* **D36** (2003) 288–293.
29. V. Gusev, *J. Acoust. Soc. Am.* **111** (2002) 80.
30. V. Gusev, *Ultrasonics* **40** (2002) 697.
31. V. Gusev, *Phys. Lett.* **A271** (2000) 100.
32. D. P. Atherton, *Nonlinear Control Engineering* (Van Nastrad, London, 1975).
33. A. Gelb and W. E. Vander Velde, *Multiple-Input Describing Functions and Nonlinear System Design* (McGraw-Hill, New York, 1968).
34. J. K. Hale, *Oscillations in Nonlinear Systems* (McGraw-Hill, New York, 1963).
35. V. Gusev, H. Bailliet, P. Lotton and M. Bruneau, *Wave Motion* **29** (1999) 211.